Motion in Cardiovascular MR Imaging[1]

Andrew D. Scott, MSc
Jennifer Keegan, PhD
David N. Firmin, PhD

Modern rapid magnetic resonance (MR) imaging techniques have led to widespread use of the modality in cardiac imaging. Despite this progress, many MR studies suffer from image degradation due to involuntary motion during the acquisition. This review describes the type and extent of the motion of the heart due to the cardiac and respiratory cycles, which create image artifacts. Methods of eliminating or reducing the problems caused by the cardiac cycle are discussed, including electrocardiogram gating, subject-specific acquisition windows, and section tracking. Similarly, for respiratory motion of the heart, techniques such as breath holding, respiratory gating, section tracking, phase-encoding ordering, subject-specific translational models, and a range of new techniques are considered.

[1] From the Cardiovascular Magnetic Resonance Unit, the Royal Brompton Hospital, Sydney Street, London SW3 6NP, England (A.D.S., J.K., D.N.F.); and the National Heart and Lung Institute, Imperial College, London, England (A.D.S., D.N.F.). Received November 15, 2007; revision requested January 15, 2008; revision received February 6; accepted March 1; final version accepted March 3; final review by A.D.S. September 2. A.D.S. supported by the British Heart Foundation. **Address correspondence to** A.D.S. (e-mail: *A.Scott07@impenial.ac.uk*).

Motion of the heart is the vector sum of three components: motion caused by the pumping action of the four chambers, motion caused by respiration, and any resulting motion from voluntary or involuntary patient movement. The latter component is usually managed in cardiovascular magnetic resonance (MR) imaging by means of patient cooperation or by means of sedation or anesthesia in pediatric and other difficult cases and will not be discussed further here.

The type and severity of image degradation induced by cardiac motion depends on the imaging sequence and parameters used, but the effects include blurring, ghosting, and misregistration (1). In addition, beat-to-beat variations in blood flow may also cause ghosting and signal loss (2). Various techniques have been devised to deal with this, including reduced echo times (3,4), gradient moment nulling (5,6), dark-blood sequences (7), dark-blood preparation (8,9), and saturation pulses (10), but these will not be further discussed. This review will concentrate on the causes of image degradation due to the motion of the cardiac and respiratory cycles, together with the strategies available to minimize the problem.

Essentials

- Despite recent developments, cardiac and respiratory motion of the heart are a problem for many cardiovascular MR studies; this motion has been extensively studied by using MR techniques.
- Artifacts due to the rhythmic pumping of the heart are generally eliminated by means of electrocardiogram gating and imaging during a window that is short relative to cardiac motion.
- Advanced techniques include tracking the imaging plane throughout the cardiac cycle and correcting blood velocities for through-plane motion.
- Methods to reduce respiratory motion artifacts include breath holding and navigator-gating performed during free breathing, which may include real-time phase-ordering, section-tracking, or subject-specific respiratory motion models.
- Recent advances include image-based registration schemes, which eliminate the need for navigator echoes and respiratory motion models.

Motion of the Heart

Cardiac-induced Motion

In the majority of cardiovascular MR sequences, data are acquired over several cardiac cycles with the assumption that motion is the same between heartbeats. This is an oversimplification, as heart motion and heart rate vary naturally on a beat-to-beat basis with respiration (11,12) and other factors. In addition, breath holding, often used in cardiovascular MR to eliminate respiratory motion, has also been demonstrated to affect cardiac activity (13).

The contraction of the heart occurs 50 to 100 times per minute in healthy subjects and is triggered by electric impulses traveling from the atria down through the ventricles to the apex, stimulating contraction of the chambers. This systolic phase begins at the electrocardiogram (ECG) R wave, and its duration is relatively heart-rate invariant, lasting around 400 msec (14). After ejection of the blood from the heart, the myocardium relaxes, forming the diastolic phase, which fills the remainder of the R-R interval.

Motion of the left ventricle (LV) in humans has been extensively examined by using tagged MR techniques (15–18). Tagging has been performed by using spatial modulation of magnetization, or SPAMM (16,19), with the displacement information and other motion parameters, such as strain (20), initially being obtained by semiautomatic tracking of the tag lines (21–24). More recently, harmonic phase, or HARP (25), postprocessing has been used to extract the motion information by applying a bandpass filter around the tagging peak in k-space and detecting the phase of the tag modulation. Alternatively, the motion information may be obtained by using displacement encoding with stimulated echoes, or DENSE (26), where the displacement encoding is obtained by using bipolar gradients in the appropriate directions. The movement of the LV may be divided into three major components during systole: longitudinal shortening, radial contraction, and opposite-hand rotation of the apex of the chamber relative to the base (Table 1).

The reduction in base-to-apex length is a result of motion of the base while the apex remains relatively stationary (27). Magnetic resonance (MR) phase velocity mapping has been used to quantify the velocity of the LV wall (28–36) (Fig 1), with such studies demonstrating maximum longitudinal velocities of around 140 mm/sec ± 40 (standard deviation) in the lateral wall during early diastole (28). Radial motion throughout the cardiac cycle in healthy subjects has been measured by Kvitting et al (30) and Petersen et al (31), with the latter reporting maximum radial velocities of 51 mm/sec at the midventricular level in the endocardium during diastole. The structure and motion of the RV has been studied to a lesser extent, but movement of the free wall is primarily longitudinal with an element of radial contraction toward the apex and anterior section (37).

Motion of the coronary arteries during the cardiac cycle has been extensively investigated by using MR techniques because of the difficulties in imaging these small highly mobile structures, which require high spatial and temporal resolution. The peak displacements in three orthogonal di-

Published online
10.1148/radiol.2502071998

Radiology 2009; 250:331–351

Abbreviations:
ARA = acceptance-rejection algorithm
ECG = electrocardiogram
LV = left ventricle
PROPELLER = periodically rotated overlapping parallel lines with enhanced reconstruction
RV = right ventricle
3D = three-dimensional
2D = two-dimensional

Authors stated no financial relationship to disclose.

rections for one such study (38) during breath holding are summarized in Table 2. The maximum displacement of the right coronary is about twice that of the left (39), with two peaks in the vessel velocity—the first in early or midsystole (during ventricular contraction) and the second in early diastole (during a fast filling period).

MR imaging of the coronary arteries relies on acquisition of data during the period of the cardiac cycle when the arteries are relatively stationary. The rest period was defined by Wang et al (40) as the longest period during the cardiac cycle during which displacement of the vessel in question is less than 1 mm in each of the superior-inferior, anterior-posterior, and left-right directions, and this has been shown to vary substantially between patients. Figure 2 plots the rest period as a function of heart rate in the right coronary artery; typically, the left coronary has a longer rest period that starts earlier (41). For both the left and right arteries,

Table 1

Motion of Ventricles in Healthy Volunteers throughout the Cardiac Cycle

Direction and Section	Base	Middle	Apex
		LV	
Radial			
Septum (mm)	4.5	4.6	4.4
Anterior (mm)	6.2	5.0	3.4
Lateral (mm)	5.8	5.5	4.5
Inferior (mm)	5.4	5.5	5.5
Longitudinal			
Septum (mm)	10.2	6.3	2.1
Anterior (mm)	10.4	6.1	1.8
Lateral (mm)	11.0	7.1	2.8
Inferior (mm)	13.1	8.2	3.6
Rotation (degrees)	−4.4	5.2	10.0
		RV	
Radial contraction			
Midventricular free wall (%)	15.8	15.9	19.5
Longitudinal contraction			
Midventricular free wall (%)	31.2	21.6	28.0

Note.—Values are means derived from several sources summarized in a review by Petitjean et al (18). Positive values indicate base-to-apex movement, radially inward movement, or counterclockwise rotation. RV = right ventricle.

Figure 1

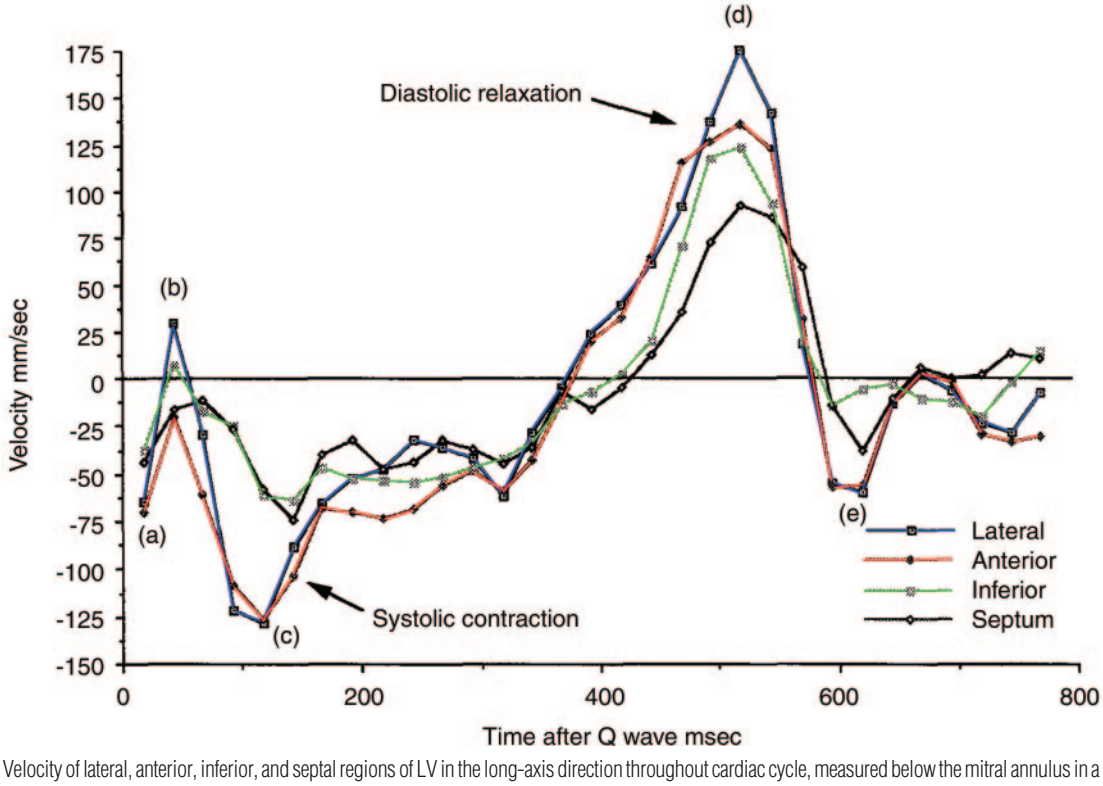

Figure 1: Velocity of lateral, anterior, inferior, and septal regions of LV in the long-axis direction throughout cardiac cycle, measured below the mitral annulus in a healthy volunteer. Initially *(a),* the heart changes from ellipsoid to spherical shape and the base moves before the relatively stationary isovolumic contraction *(b).* Base moves toward the apex during systole *(c),* away from the apex during diastole *(d),* and finally back toward the base *(e).* (Modified and reprinted, with permission, from reference 28.)

the motion tends to slow gradually before this period and to accelerate rapidly afterward. The onset of the rest period has been established as approximately 750 msec after the R wave of the ECG (40), although in some cases a relatively longer rest period may be present starting at end systole (42), particularly when the R-R interval is short (43). The duration and the time to onset of the rest period following the R wave may be increased by using a β-blocker (43).

Respiratory-induced Motion

In healthy individuals, respiratory motion may be comfortably suspended for 20–30 seconds by means of breath holding. However, Holland et al (44) report that the left heart margin at the heart base may drift 2.7 mm or more during inspiration before breath holding and 1.1 mm or more during expiration (quoted, as in other reports in this section, for a single time point in the cardiac cycle). They suggest that the heart rate increases toward the end of the breath hold. Jahnke et al (43) found that in 33% of patients, the diaphragm position was irregular and unsteady or drifted continuously during breath holding.

It should be further noted that inspiratory and expiratory breath-hold positions do not generally correspond to the free-breathing end-inspiratory and end-expiratory equivalents. Tidal breathing involves motion of the chest wall and diaphragm, both of which influence the motion of the heart. The relationship between the motion of the heart and the superior-inferior motion of the diaphragm is approximately linear (45,46) although highly subject specific (47), with an element of hysteresis (Fig 3). Taylor et al (48) recorded, in nine healthy subjects, end-inspiratory and end-expiratory dwell times during free breathing of 1.1 seconds ± 1.6 and 0.4 second ± 0.2, respectively, with a respiratory period of 4.3 seconds ± 1.1 , diaphragmatic amplitudes of 14.1 mm ± 4.8 and maximum inspiratory and expiratory velocities of 13.3 mm/sec ± 5.3 and 11.8 mm/sec ± 4.8, respectively. McLeish et al (49) studied respiratory-induced motion of the heart with both rigid and nonrigid transformation parameters generated at various breath-hold positions (Table 3) and demonstrated that the largest component of motion is in the inferior direction during inspiration, with the large standard deviations suggesting high intersubject variability. Much smaller equivalent displacements and rotations recorded during free-breathing conventional coronary angiography (50) may be partially accounted for by the large range of diaphragm displacements (up to 40 mm) found by McLeish et al (49), suggesting that the breath-hold positions used were not in the range of normal tidal breathing (around 14 mm [48]).

Table 2

Maximum Displacement of Coronary Arteries in the Cardiac Cycle during Breath Holding

Artery	Left-Right (mm)	Anterior-Posterior (mm)	Superior-Inferior (mm)
Left anterior descending	6.8 ± 1.7	7.9 ± 1.5	6.8 ± 1.9
Left main	7.9 ± 1.3	9.0 ± 1.7	7.1 ± 1.3
Left circumflex	9.3 ± 2.1	12.7 ± 2.3	10.5 ± 1.3
Proximal right coronary	9.0 ± 1.7	10.6 ± 1.7	11.3 ± 2.8
Distal right coronary	12.6 ± 2.2	16.7 ± 2.9	10.3 ± 2.4

Note.—Data are mean ± standard deviation in eight healthy volunteers. Adapted and reprinted, with permission, from reference 38.

Figure 2

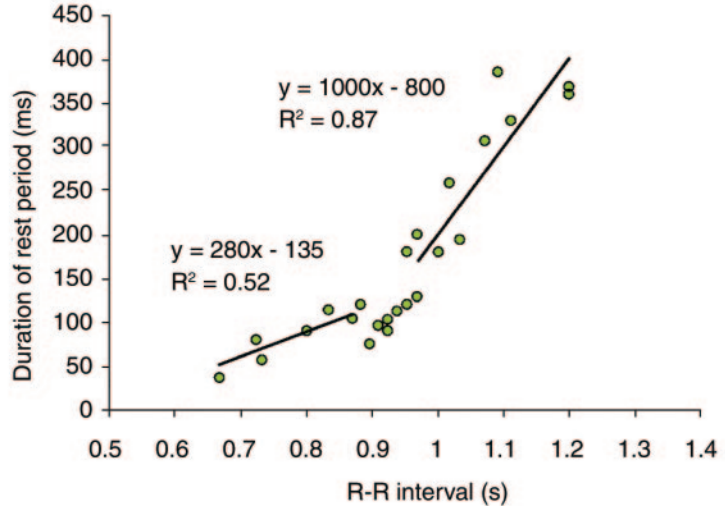

Figure 2: Graph shows data from 25 healthy volunteers for duration of right coronary artery rest period as a function of R-R interval, as measured in a plane perpendicular to direction of flow. Linear regression equations for long and short R-R intervals are shown. (Reprinted, with permission, from reference 41.)

Dealing with the Motion

Motion from the Cardiac Cycle

Cardiac gating.—With the advent of rapid MR imaging techniques, it is now possible to acquire single-shot real-time images without ECG gating, as has been used in interventional MR applications (51–53), rapid assessment of LV function (54), and angiography and flow measurement (55–58). Compromises are made, however; with most techniques, image data are acquired over a number of cardiac cycles with the requirement that the data acquisition be

triggered. Triggering may be achieved by using pulse oximetry (59), laser Doppler velocimetry, or plethysmograph peripheral pulse monitoring (60). ECG information is preferable, because *(a)* the former techniques are unable to trigger from the beginning of the cardiac cycle, *(b)* there are variable delays from the R wave to the trigger, and *(c)* motion artifacts can be generated with the former techniques (60,61).

Several investigators (62–68), however, have directly extracted information on the cardiac phase from MR data for gating or motion compensation. A subgroup of such techniques, known as cardiac self-gating (66–68), derive an ECG-like signal from cardiac-induced periodic variations in a line of k-space repeatedly acquired without phase encoding. This information may be used in a similar manner to the ECG data, without the need for careful electrode placement or potentially hazardous metallic conductors in the magnet bore. ECG gating, however, remains the most commonly used technique, as such alternatives require rapid online processing and are not easily implemented. Further developments in ECG gating include algorithms used with vector cardiograms (69), which increase the accuracy of R-wave detection in the presence of magnetic field distortions and artifacts due to gradient switching, radiofrequency pulses, blood flow, and motion. ECG-gated acquisitions can also be improved in some cases by implementing arrhythmia-rejection algorithms (70) that exclude data acquired during R-R intervals that deviate by more than −10% or +50% from the average period of the last eight accepted intervals. Implementation of these techniques, however, can result in an increased and unpredictable imaging duration, which may be a problem for studies acquired during a breath hold.

There are two ways of using the ECG information to gate data acquired throughout the cardiac cycle. Prospective gating uses the R wave from the ECG to initiate the acquisition of the image data. A group of k-space lines (or a segment) is acquired repeatedly in each R-R interval (71) to cover 80%–90% of the cardiac cycle. Data are acquired until k-space is sufficiently sampled. The number of segments acquired per cardiac cycle equals the reconstructed frame rate and is dependent on the sequence repetition time and the heart rate. The advantage of this technique is that only the required data are collected. The disadvantage, however, is that, to allow for natural variability in the R-R interval, the final 10%–20% of the R-R window (72) is not included in the acquisition window (while the system is waiting for the next R wave). A further issue is that this "dead time" disturbs the steady state and leads to increased signal intensity in the first few frames when a conventional gradient-echo cine sequence is used (73), referred to as the "lightening artifact," and to other artifacts when a balanced steady-state free precession sequence is

Figure 3

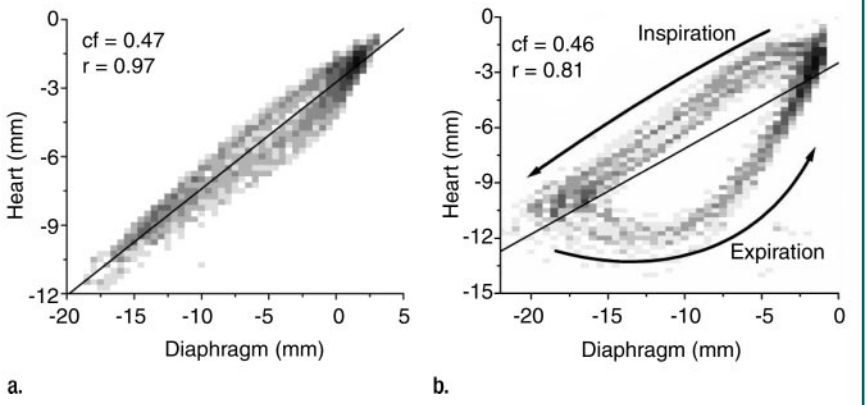

Figure 3: Graphs show superior-inferior respiratory-induced motion of LV versus that of right hemidiaphragm in two volunteers, **(a)** one with mild hysteresis and **(b)** one with substantially more. Darker squares indicate that this result measurement was more common. The direction of the hysteresis was always found to be counterclockwise (arrow). *cf* = Correction factor (ie, tracking factor), *r* = correlation coefficient. (Adapted and reprinted, with permission, from reference 46.)

Table 3

Whole-Heart Rigid Transformation Parameters and Selected Point Displacements between End Expiration and End Inspiration

Parameter	Breath Hold	Free Breathing*
Right-left translation (mm)	3.8 ± 1.2	−0.4 ± 2.2
Anterior-posterior translation (mm)	7.1 ± 2.9	1.1 ± 1.9
Superior-inferior translation (mm)	16.4 ± 4.2	4.9 ± 1.9
Right-left rotation (degrees)†	1.8 ± 1.7	1.6 ± 0.9
Anterior-posterior rotation (degrees)†	3.8 ± 1.8	1.1 ± 1.9
Superior-inferior rotation (degrees)†	−0.6 ± 3.3	0.4 ± 2.2
Right atrium midpoint displacement (mm)	16.0 ± 4.2	NA
Right coronary artery midpoint displacement (mm)	17.0 ± 4.0	NA
LV apical point displacement (mm)	22.5 ± 4.2	NA
Right hemidiaphragm displacement (mm)	42.7 ± 11.2	NA

Source.—References 49 and 50.

Note.—Data are mean ± standard deviation. Positive displacement is toward the left, posterior, or inferior direction. Free-breathing data were acquired with conventional angiography; breath-hold data, with MR imaging.

* NA = not applicable.

† Angle is around the given axis (right-left, anterior-posterior, or superior-inferior).

used. These artifacts may be eliminated, however, with the use of dummy radiofrequency and gradient pulses during the dead time.

Retrospective gating can be achieved in two ways (72). A segment of k-space may be repeatedly acquired through the R-R interval and moved to the next segment on the fly when the next R wave is detected. Alternatively, the acquisition may be asynchronous with the ECG, so that a segment is acquired for a fixed number of repetitions. In the latter approach, each repeated segment covers approximately 125% of the R-R interval to allow for heart rate variation, and each segment is labeled with the corresponding cardiac phase from the ECG. Once all segments are acquired, the data are reordered before reconstruction. The main advantage of these techniques is that data can be acquired throughout the entire cardiac cycle, helping prevent the underestimation of both the atrial (74) and ventricular (72) ejection fractions and volumes that are demonstrated with prospective triggering techniques. Furthermore, they are less sensitive to irregular heartbeats and have reduced systematic noise and blurring (73). The latter retrospective method benefits from the constant number of segments acquired and has traditionally been easier to implement (73). It is, however, more time consuming owing to the 25% oversampling factor, which results in longer breath holds or reduced spatial resolution.

Figure 4

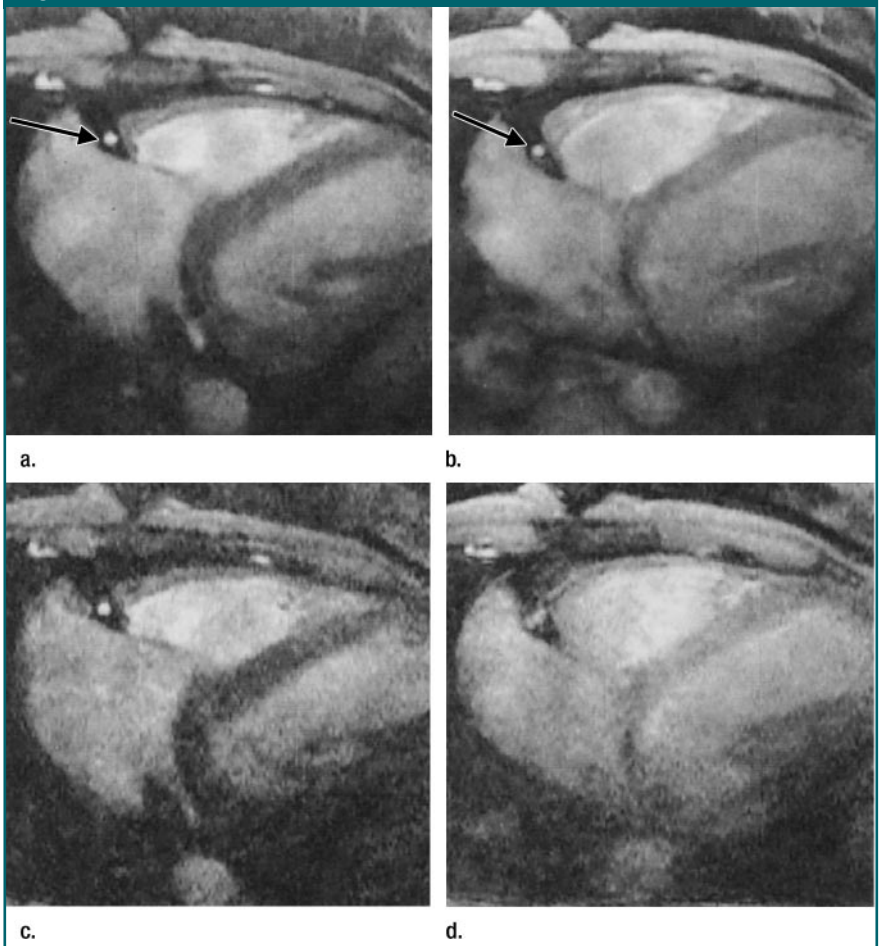

Figure 4: **(a–d)** Magnitude MR images from phase-velocity mapping study of right coronary artery (arrow) in a healthy volunteer during **(a, c)** middiastole (when the heart is relatively stationary) and **(b, d)** early systole (during rapid cardiac motion). Images were acquired with **(a, b)** retrospective respiratory gating with an oversampling factor of eight and acquisition window of 32 msec and **(c, d)** during breath holding with acquisition window of 126 msec. In diastole, retrospective respiratory-gated and breath-hold studies both result in good quality images. In systole, rapid cardiac motion and long acquisition window result in considerable motion blurring of the artery. (Adapted and reprinted, with permission, from reference 75.)

Selection of the acquisition window.—When imaging throughout the cardiac cycle is required, a compromise needs to be made between the number of frames acquired and the acquisition duration for each frame. Although acquisition of multiple data segments per cardiac cycle increases the acquisition window for each frame and decreases the temporal resolution of the study, it has the benefit that the study is completed more quickly. However, if the acquisition window is long, motion blurring will occur (Fig 4) (75).

For imaging at a single time point in the cardiac cycle in applications such as coronary artery imaging, prospective triggering is normally used to acquire a number of k-space lines in a time that is short with respect to cardiac motion. The heart is relatively still during the middle of the diastolic phase of the cardiac cycle, which is most often used as the acquisition window, although it is possible to image during systole (76).

Empiric suggestions for the delay from the R wave to the onset of the optimum acquisition window in middiastole are based on measurements of the length of the systolic phase and include 350 msec (77) and 550 msec − 0.002 · HR, where HR is heart rate (in beats per minute) (14,78). However, there is large variability between subjects in both the onset and the duration of the rest period (39,40), and the best approach, particularly for high-resolution imaging, is to tailor the acquisition parameters to the individual patient.

In coronary imaging, the optimal timing and duration of the acquisition window are determined in a "prescanning" stage, either by using a repeated one-dimensional MR acquisition (78) or from a cardiac motion study (40,41) with the use of long acquisition windows

in subjects with a slow heart rate, resulting in an increased imaging efficiency without detriment to image quality (40,79). Alternatively, the trigger delay and, potentially, the acquisition window may be adjusted in each cardiac cycle on the basis of the average duration of previous R-R intervals and information from prescanning that have been input into a generic model (80). Another approach, implemented by Wang and Ehman (81) and called cardiac motion–matched k-space sampling, acquires the central lines of k-space (which are more sensitive to motion) during the period of minimum motion in diastole and the outer lines of k-space during less stationary periods. As a result, Wang and Ehman were able to extend the cardiac acquisition window (333 msec vs about 100 msec) for contrast material–enhanced three-dimensional (3D) coronary MR angiography and, consequently, increase imaging efficiency. Alternatively, the acquisition window may be extended by acquiring multiple image segments per cardiac cycle and using intersegment motion correction based on epicardial fat tracking (82).

Selection of the acquisition window is also important in morphologic imaging of the heart with dark-blood–prepared turbo spin-echo sequences, which use a double inversion pulse to null blood signal and, optionally, a further inversion pulse to null fat signal (83). The delay after the double inversion pulse must be adjusted to null signal from blood and to avoid signal drop out from misregistration of the myocardium between the dark-blood preparation (immediately after the R wave) and imaging (in the diastolic rest period of the same cardiac cycle). Misregistration errors can, in part, be reduced by increasing the section thickness of the double inversion pulse preparation, although this can reduce the effectiveness of the dark-blood suppression, particularly in the presence of slow-moving blood. Alternatively, Keegan et al (84) offset the section-selective component of the preparation pulses from the imaging plane to take into account the expected motion of the myocardium and demonstrated reduced signal loss.

Figure 5

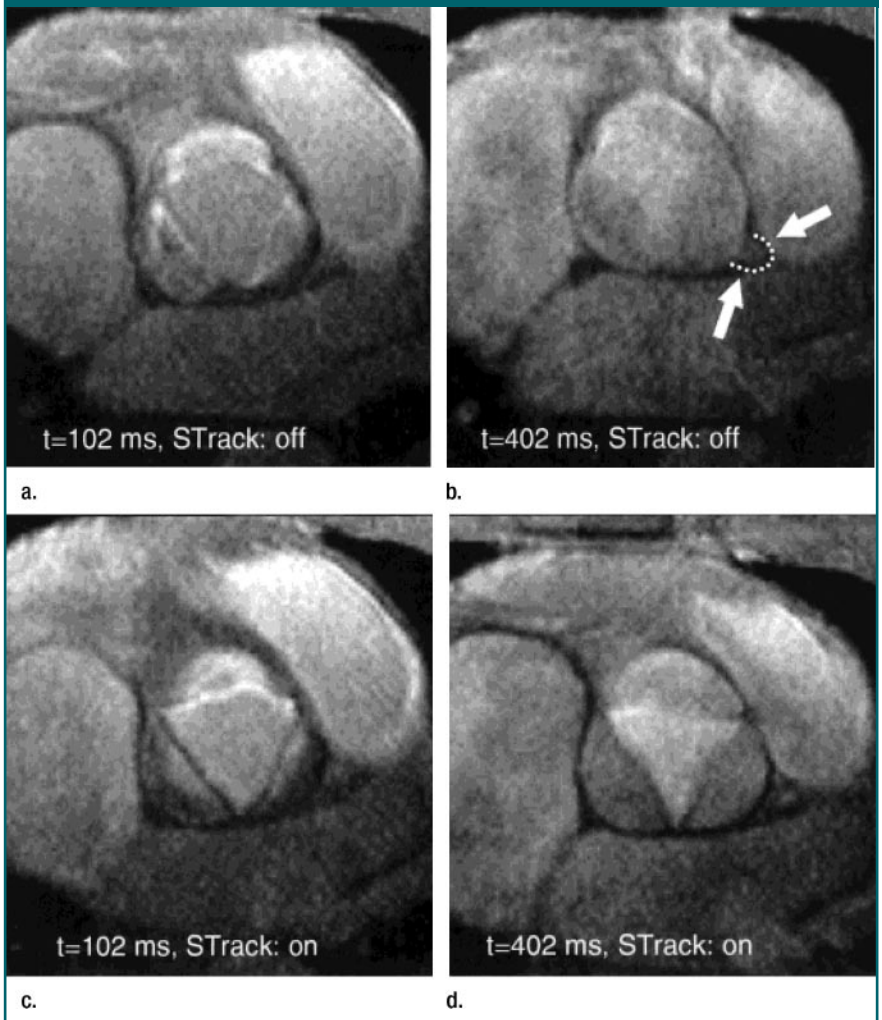

Figure 5: **(a–d)** Magnitude MR images of cross section of aortic valve at two time points *(t)* in the cardiac cycle, with and without section tracking *(STrack)*. Section tracking enables valve to be seen with greater clarity at both time points. Arrows in **b** highlight left coronary root, which has moved into the imaging frame since **a** but is rightly absent in **d.** (Reprinted, with permission, from reference 85.)

Section tracking and motion compensation through the cardiac cycle.—When images must be acquired throughout the cardiac cycle (or outside of the diastolic rest period), one method of dealing with cardiac motion is to change the orientation and offset of the image plane to follow the motion of relevant anatomy. The motion of relevant anatomy may be automatically extracted from a single prescan with labeling of the plane of interest (85). It should be noted that those structures not moving with the plane of interest will generate ghosting artifacts. Kozerke et al (85) used this technique to label the basal short-axis plane in the ventricles, which improved cine phase-velocity mapping of flow through the aortic valve and enabled better delineation of the valve leaflets (Fig 5). Similarly, this method was used to assess aortic and mitral valve regurgitation (86) and to generate the 3D morphology of the aortic valve throughout the cardiac cycle (87).

In an extension of this approach, Dowsey et al (88) replaced the selective component of the labeling prepulse with a comb (series of delta functions) exci-

tation (89) to enable the simultaneous labeling of multiple parallel planes. They used the subsequent motion information to image detail in the ventricular trabeculations and for strain analysis.

This approach has also been used in morphologic imaging of the heart with dark-blood–prepared turbo spin-echo imaging to track the motion of the plane of interest among the dark-blood preparation, an optional short tau inversion-recovery preparation pulse, and the imaging phase of the acquisition (84). The results showed reduced signal drop out from misregistration and improved image quality, as compared with nontracked imaging, particularly in the highly mobile basal short-axis plane (Fig 6). Such approaches could also potentially be applied to track the motion of the heart by using techniques with long acquisition windows, such as myocardial perfusion sequences.

A related technique has been applied to tagged imaging of the myocardium (90), where a thin section of tissue is excited with in-plane tags, and a much larger volume, certain to contain the excited section, is imaged. The thin section is imaged despite movement in the through-plane direction, and the information from the tags may be used for assessment of in-plane motion, including strain estimation.

Phase-velocity mapping of blood flow in the heart could also be corrected for the motion of the heart itself, although in practice the motion of the heart is small relative to the motion of blood flow, and the correction is usually ignored. In measuring the low flow velocities present with valvular regurgitation by using phase-velocity mapping, however, such a correction is desirable. Kayser et al (91) subtracted the velocity of a ring of tissue in the tricuspid annulus from the blood flow measurements through the tricuspid valve and demonstrated significantly different results for three of eight parameters describing RV function. Alternatively, in the previously described work by Kozerke et al (85), the velocity of the aortic valve (derived from a tagged prescanning acquisition) was subtracted from the measured velocities and was found to be more reliable.

For coronary flow assessment where the through-plane velocity of the blood vessel may be comparable to the velocity of blood flow in the vessel itself, correction is essential. In the left coronary artery, correction can be performed by subtracting the measured velocity of an adjacent region of myocardium (92). This technique has also been applied to flow measurements in the right coronary artery (93) but is generally difficult because the neighboring myocardium is thin and poorly defined. Keegan et al (94) devised an alternative approach using the epicardial fat that surrounds the arteries as a marker of the velocity of the vessel (Fig 7). In their study, interleaved spiral fat- and water-velocity–mapped images were obtained in a single acquisition, and flow velocity curves in both right and left coronary arteries were comparable to those found by using a Doppler guidewire.

Respiratory Motion

Simple breath holding.—Early cardiovascular MR examinations were performed during free breathing with no respiratory motion compensation (95–97). Subsequent improvements in imager technology and sequence design have enabled many studies to be completed within a single breath hold (98) (usually at end expiration, which is more stable and reproducible and blood flow is similar to that during free breathing [99]).

For many applications, however, studies cannot be completed with sufficient signal-to-noise ratio or resolution within the comfortable breath-hold period of 20–30 seconds for a healthy volunteer (less for many patients). One alternative is to use multiple breath holds (100) and to acquire segments of k-space or a subset of sections in each; but if breath-hold reproducibility is poor, misregistration artifacts may result. Some investigators (101) have registered multiple breath-hold short-axis volumes to a breath-hold long-axis volume to correct for misregistration between short-axis volumes. Others (102–104) have extended breath-hold dura-

Figure 6

Figure 6: **(a–c)** Dark-blood T2-weighted short tau inversion-recovery turbo spin-echo MR images of basal short-axis plane in a healthy volunteer, with and without section tracking. **(a)** Untracked conventional, **(b)** LV-tracked, and **(c)** RV-tracked acquisitions. In **b** and **c,** section-selective preparation pulses (dark-blood and short tau inversion-recovery) are positioned to take into account motion of ventricle of interest between preparation and imaging phases. (Adapted and reprinted, with permission, from reference 84.)

Figure 7

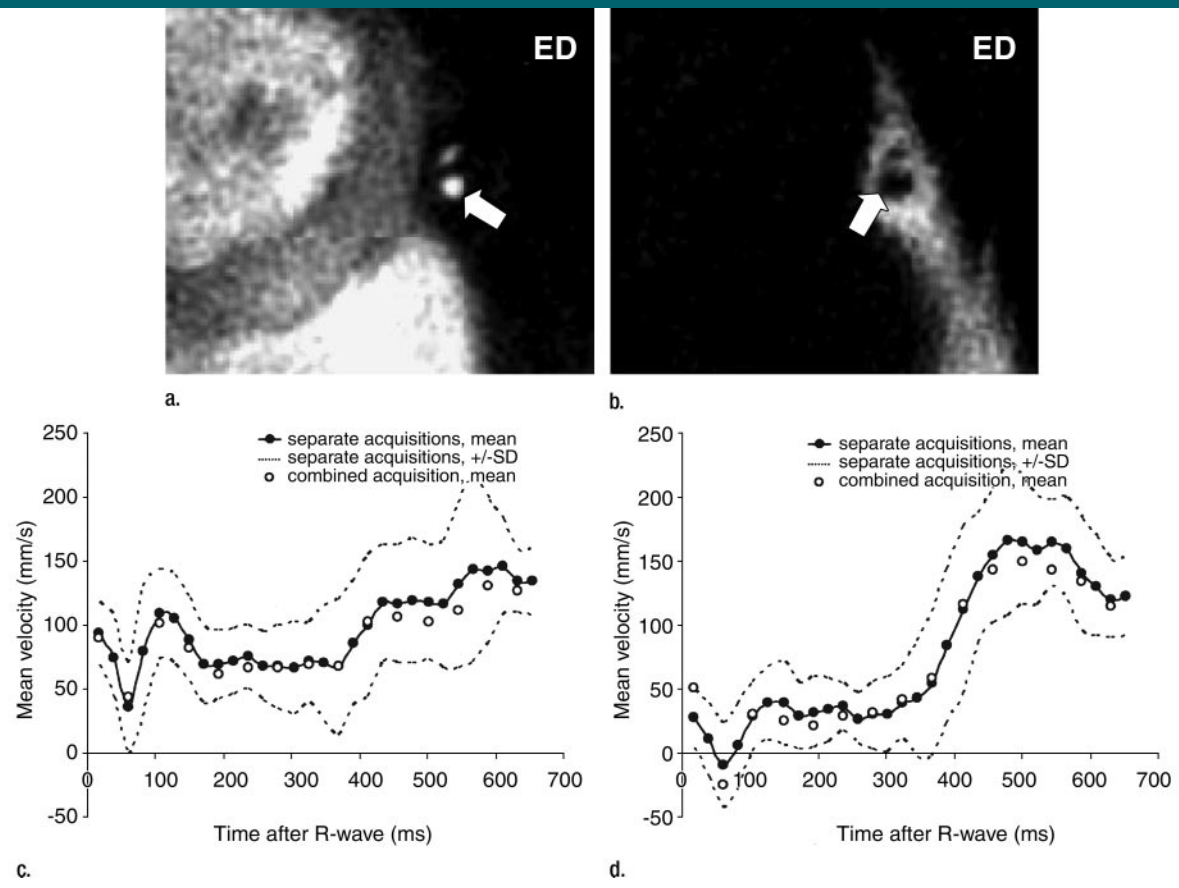

Figure 7: **(a, b)** Spiral phase-velocity MR mapping of left anterior descending artery (arrow) in a healthy volunteer at end diastole *(ED)* with **(a)** water- and **(b)** fat-selective excitation. **(c, d)** Graphs show mean velocity through cardiac cycle derived from water-selective excitation in 13 healthy subjects **(c)** uncorrected and **(d)** corrected for through-plane motion of artery by subtracting velocity of surrounding fat to give expected diastolic predominant left anterior descending artery flow velocity profile. Fat and water acquisitions were performed both as separate acquisitions (●) to maintain temporal resolution and by interleaving both acquisitions within cardiac cycle (○) to maintain overall imaging duration. *SD* = standard deviation. (Adapted and reprinted, with permission, from reference 94.)

tion by using supplementary oxygen or hyperventilation. Danias et al (105) extended breath holds by 40% by using hyperventilation, 24% by using supplemental oxygen, and 59% by using hyperventilation and oxygen. However, all breath-holding schemes require patient cooperation, which can be problematic and may cause image quality to suffer as a result of respiratory drift during the respiratory period (105).

Monitoring respiration.—Various methods for monitoring respiration have been suggested along with ways of gating, triggering, or compensating for the motion detected. Systems to monitor the motion of the chest wall include belts across the patient (106), electric impedance between ECG electrodes (107), bellows (108,109), or optical compression devices (110). Methods to monitor the expired and inspired gas involve capnography, temperature sensors in oxygen masks or nasal cannulas (106), and spirometers. Techniques to monitor the diaphragm include navigators, discussed below, and ultrasonography performed during the cardiovascular MR examination (111). The biggest disadvantages of these systems, however, are poor patient tolerance and the assumptions made about the relationship between the output signal and the motion of the heart.

Methods in which MR data are used are generally known as navigator techniques. The most common forms involve a column of tissue excited by using either a two-dimensional (2D) spiral-like radiofrequency pulse (112) or a section-selective 90° radiofrequency pulse followed by a noncoplanar 180° section-selective pulse (113). The former has the disadvantages of requiring a complex radiofrequency pulse and may have a poorly defined excitation profile in regions of poor shim, whereas the latter is more robust but causes saturation artifacts if either of the excitation planes intersects the imaging volume. In either case, a frequency-encoding gradient is

applied along the length of the excited column to provide a profile through the moving structure of interest. This type of navigator may be placed on the chest wall, directly on the heart, or on the diaphragm, with the peak of the dome of the right hemidiaphragm being the most common position for ease of setup and sharpness of the diaphragm edge (77,109). The position of the diaphragm, clearly delineated by the liver-lung interface on the right hemidiaphragm can be extracted from the reconstructed navigator profiles by using either edge-detection (114), correlation, or least-squares methods. Wang et al (115), however, suggests that the edge-detection method is unsuitable for use with most navigator profiles except those that use external markers, due to an insufficient signal-to-noise ratio and edge definition. However, a similar technique developed by Du et al (116) improves this by smoothing and thresholding the navigator profiles.

The other two techniques are more computationally demanding, with the least-squares technique shown to be more robust in the presence of noise and profile deformation (115). The signal-to-noise ratio of the navigator signal, and hence the accuracy of the derived information, may also be affected by preparatory pulses in the sequence. In the case of double-inversion dark-blood preparation for vessel wall imaging and cardiac morphology, an additional reinversion pulse is often applied to the column of tissue used for the navigator signal to restore the signal-to-noise ratio (117). One navigator is typically acquired before, after, or on either side of the imaging segment every R-R interval. Rapid processing of the navigator and feedback to the imaging sequence are essential for prospective correction. Spuentrup et al (118) demonstrated a significant increase in image quality for high-resolution 3D coronary MR angiography when the time from navigator echo to acquisition window was decreased from 100 to 20 msec.

Use of displacement information to guide and gate acquisitions.—Prospective techniques can only be used with respiratory information acquired prior to the acquisition window in the cardiac cycle and, as mentioned earlier, require rapid processing and feedback of the respiratory signal. Alternatively, retrospective techniques are used. With the original retrospective respiratory gating technique (119), each line or segment of k-space was acquired multiple times (typically, a factor of five was used). The modal respiratory position was determined from a histogram of the respiratory data stored with the image data, and the reconstruction was performed with data acquired over the minimum range of diaphragm positions around the mode. Although this approach decreased the range of motion present in the final image, the degree of motion could still be large in the presence of respiratory drift, and the low respiratory efficiency (the proportion of acquired data accepted for reconstruction, 20% in this case) was such that this technique would only be used if prospective methods were not possible.

Prospective techniques have been used to acquire data over multiple consistent breath holds or during free breathing. In the former, the navigator position is fed back to the subject by a visual (114,120) or audible indicator (108) and is used to guide the breath-hold position. The acquisition starts after the subject has suspended respiration within an operator defined window after a short settling period (121). Alternatively, Chandler et al (122) registered 2D short-axis images from multiple breath holds to a 3D transverse volume. Although techniques such as these have been successful in increasing inter–breath-hold reproducibility in studies of healthy volunteers, the cooperation required from patients is prohibitive in the majority of cases (123).

The prospective acceptance-rejection algorithm (ARA) (124,125) reconstructs free-breathing data acquired when the respiratory signal lies within a user-determined window around a reference position, typically end expiration (Fig 8). Larger gating windows clearly result in more data being accepted, and hence a higher respiratory efficiency but also lead to reduced image quality. Wang et al (121) used two navigator echoes per cardiac cycle, one placed temporally on either side of the image segment, to reject and reacquire data acquired with high intrasegment motion. In contrast to the retrospective respiratory gating technique, with ARA the image is acquired with a predefined range of motion but an undefined imaging duration.

Although early ARA studies demonstrated similar results to those of breath holding (125), temporal changes in breathing patterns during data acquisition are frequent and may result in a drastic loss of respiratory efficiency and ghosting (48). Additional techniques are

Figure 8

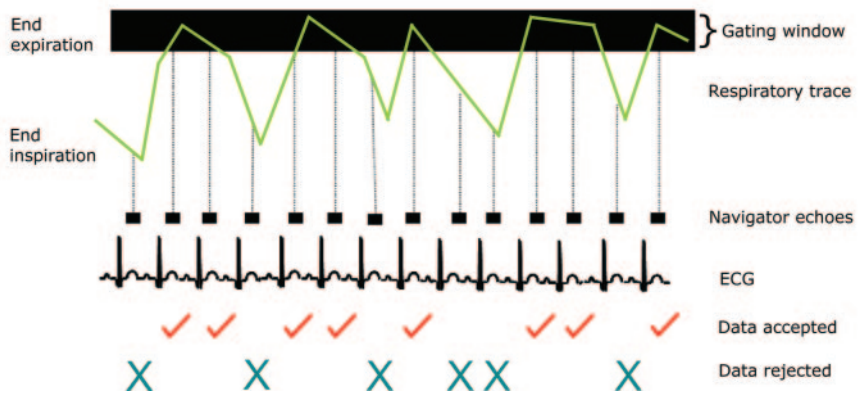

Figure 8: Schematic shows ARA. If respiratory trace lies within predefined user-selected gating window, the immediately following image data are accepted and used in reconstruction; otherwise, the data are rejected and reacquired in next cardiac cycle.

often employed in combination with ARA to improve respiratory efficiency and/or image quality.

Methods to Improve Respiratory Efficiency in Prospectively Gated Free-breathing Acquisitions

An approach that may be implemented to improve respiratory efficiency and/or image quality is to implement real-time k-space ordering that depends on the phase of the respiratory cycle. k-Space ordering techniques rely on the fact that movement during acquisition of the outer k-space lines is less detrimental to image quality than the same movement during the acquisition of the central k-space lines (126).

Various algorithms exist. One is respiratory-ordered phase encoding (ROPE) (110), where phase-encoding lines are ordered as a slowly varying function of diaphragm position. Another is centrally ordered phase encoding (COPE) (127), where the central region of k-space is acquired at end expiration, and the remaining lines are acquired symmetrically around the center of k-space. Similarly, in hybrid ordered phase encoding (HOPE) (128), the center of k-space is acquired at the most common diaphragm position, and, by using a histogram of respiratory positions, areas of k-space are distributed to histogram bins, thereby maintaining the monotonic relationship of respiratory position and phase-encoding line used in ROPE. This work was extended to 3D imaging and improved by using a dual gating window of 5 mm for the central 75% of k-space and 10 mm for the remainder. This was shown (129) to maintain image contrast and resulted in much improved respiratory efficiency in comparison to images of equivalent quality acquired with ARA (72% vs 48%).

A number of techniques not requiring a gating window potentially reduce the problems associated with respiratory drift. With the diminishing variance algorithm (130), a complete set of data is initially acquired during free breathing, and the modal diaphragmatic displacement is determined from a histogram. During the remainder of the acquisition, in each R-R interval the segment previously acquired at the greatest diaphragm displacement is reacquired, efficiently reducing the variance of the diaphragm displacements. Acquisition is terminated when the variance drops below a predefined cutoff or when a predefined time limit is exceeded but sufficient data exist to reconstruct an image at any time point following the acquisition of the initial data set. This technique has been extended to 3D imaging (131) by using three orthogonal navigators (superior-inferior over the right hemidiaphragm, anterior-posterior on the chest wall, and left-right on a posterior region of the heart), and it was shown that the anterior-posterior data were useful, but the right-left data were less so.

In another technique, motion-adapted gating (132), phase-encoding lines are acquired according to a weighting function that varies with diaphragm displacement. The respiratory phase obtained from each navigator is used to determine which phase-encoding lines may be acquired, and the line closest to the center of k-space that has not yet been filled is obtained. In an extension to this technique, if all lines permitted by the weighting function have been acquired for the current diaphragm position, the measurement may be used to improve the data acquired at a k-space line with a greater displacement. In a further development, Sinkus and Börnert (133) used a weighting function equivalent to a dual gating window through k-space. Rather than generate the reference point (or "seed") for the acquisition from an initial prescan, the acquisition is started by obtaining random phase-encoding lines, which may aid the later reconstruction, while generating the seed. Parameters indicating the image quality if the acquisition was to be prematurely terminated and the remaining imaging duration are generated to influence decisions on whether to stop the acquisition or to shift the seed position when respiratory drift occurs.

Phase ordering with automatic window selection (PAWS) is an alternative technique aimed at combining the advantages of the diminishing variance algorithm and ARA. The respiratory signal range is binned, and each bin is assigned a starting point in k-space. Once three adjacent bins covering k-space are fully acquired, data are reconstructed with a maximum respiratory displacement range of the combined bin widths. Three-dimensional motion-adapted gating (134) extends the PAWS technique to 3D. When applied to coronary artery imaging, results were comparable to ARA navigator gating with markedly improved imaging efficiency (135).

Section tracking and motion correction.—Several techniques improve respiratory efficiency by correcting for the measured motion within a larger gating window. The retrospective technique, adaptive navigator correction suggested by Ehman and Felmlee (113) and later implemented for 3D imaging (136), applies a phase shift to the measured data that is dependent on navigator-measured diaphragm position. More recently, Wang and Ehman (81) used a similar retrospective technique with linear interpolation of the respiratory signal between the pre- and postimaging segment navigators to correct 3D coronary imaging data. The results demonstrated similar image quality with an 8.4-mm gating window and correction when compared with an ARA-gated study with a 2.8-mm window.

Both retrospective and prospective correction techniques require accurate tracking factors to relate the motion of the heart to that of the diaphragm. As discussed previously, this relationship is approximately linear, although it is not one to one. Wang et al (45) assumed rigid body motion of the heart and related the position of the midpoint of the left hemidiaphragm on 2D coronal and sagittal images to that of various landmarks in the heart during breath holds at different inspiratory positions. These results have led to the section-tracking factors that are in common use of 0.57 in the superior-inferior direction and 0.09 in the anterior-posterior direction.

McConnell et al (137) used these values in developing the prospective section-tracking technique for the coronary arteries with multiple guided

breath holds. Section tracking prospectively shifts the imaging volume in each R-R interval by an amount determined by the section-tracking factors and the respiratory motion signal. Danias et al (112) extended this prospective technique to free breathing, correcting for motion within a navigator gating window by using the superior-inferior and anterior-posterior tracking factors from Wang et al (45). They found that section tracking enabled an increase in the gating window from 5 to 7 mm, with an increase in respiratory efficiency but without a discernable loss in image quality when compared with images acquired with the ARA technique using a 5-mm window. Extending the gating window further and using the same section-tracking factors resulted in a decrease in image quality, however, highlighting the inadequacy of such a non–subject-specific and simple model. In many studies (117,138–141), only a superior-inferior correction was used and the navigator was applied at the right hemidiaphragm (as discussed previously) during free breathing; yet in the original work, Wang et al (45) used breath holding and the left hemidiaphragm as a reference. During breath holds, the relationship between chest wall and abdominal motion may change relative to that during free breathing; thus, when deriving tracking factors from multiple breath holds, it is likely that a larger range of diaphragm positions are used than occur during normal tidal breathing.

In addition to the differences in location and technique for measuring diaphragm displacement, this may account for the inconsistencies in average tracking factors between studies (45,47,103,142) (Table 4). These studies, however, report large standard deviations, suggesting high intersubject variability. The subject dependence of the section-tracking factor may be partly resolved by calculating a subject-specific tracking factor in the superior-inferior direction (47,143,144). Taylor et al (47) used both two-point (inspiration and expiration) and seven-point (navigator-guided) breath-hold images to relate right hemidiaphragm movement to that of the coronary arteries in the superior-inferior direction. They demonstrated that improved image quality was maintained when subject-specific tracking was used and the gating window was increased from 6 to 16 mm.

A potential problem with all motion-correction techniques is the artifact generated by structures not moving with the region of interest. This may be reduced by applying spatial saturation bands over static structures such as the chest wall. Alternatively, Yang et al (145) described a zonal imaging technique whereby a 2D radiofrequency pulse is used to excite a restricted region of tissue for 3D imaging. The advantages of such a technique are that imaging time is reduced because fewer phase-encoding lines are required to sample the excited region, and stationary structures not within the excited region do not generate artifacts. Gatehouse et al (120) used this technique with a 20-mm gating window and subject-specific tracking in the superior-inferior and anterior-posterior directions to demonstrate image quality similar to that obtained with navigator-guided breath holds with a 5-mm gating window, resulting in an improvement in mean respiratory efficiency from 61% to 95%.

Besides the intersubject variability of linear tracking factors, the motion of the heart during respiration is not that of a rigid body, and hysteretic effects (46,146) are seen between inspiration and expiration (Fig 3). A recent approach to handling this has been to develop subject-specific prospective respiratory motion models, in which the motion of the heart is modeled as a 2D or 3D translation or as an affine transformation (146–150), including linear scale, shear, and rotation in addition to 3D translation. The nonrigid parame-

Table 4

Section-tracking Factors Relating Motion of Different Regions of the Heart to Superior-Inferior Motion of the Diaphragm

Study and Tracking Factor*	Tracked Location†	Imaging Method†
Wang et al (45)		Two perpendicular sections including LHD and heart, with breath holding
0.57/0.09/NR	RCA root	
0.70/0.85/NR	Proximal LAD	
0.81/0.07/NR	Apex	
0.62/NR/NR	SHM	
0.92/NR/NR	IHM	
Danias et al (103)		RHD and coronary arteries in same section during free breathing
0.6/NR/NR	Left MCA	
Taylor et al (47)		Navigator on RHD and imaging of heart during breath holding
0.49/NR/NR	Proximal RCA	
0.59/NR/NR	Proximal LCA	
Nagel et al (143)		Imaging of RHD and heart in separate section during breath holding
0.62/NR/NR	ILV	
0.27/NR/NR	LCA	
Keegan et al (142)		Navigator on RHD and imaging of RCA during free breathing
0.25/0.04/0.12	RCA root	
Fischer et al (146)		Navigator on RHD and imaging of heart during free breathing
0.38/NR/NR	Proximal RCA	
0.59/NR/NR	Distal RCA	
Jahnke et al (150)		Navigator on RHD and 3D imaging of heart during free breathing
0.45/−0.01/0.02	Whole heart	

* Tracking factors are listed as superior-inferior/anterior-posterior/left-right. NR = not reported.

† IHM = inferior heart margin, ILV = inferior LV wall, LCA = left coronary artery, LHD = left hemidiaphragm, MCA = main coronary artery, RCA = right coronary artery, RHD = right hemidiaphragm, SHM = superior heart margin.

Figure 9

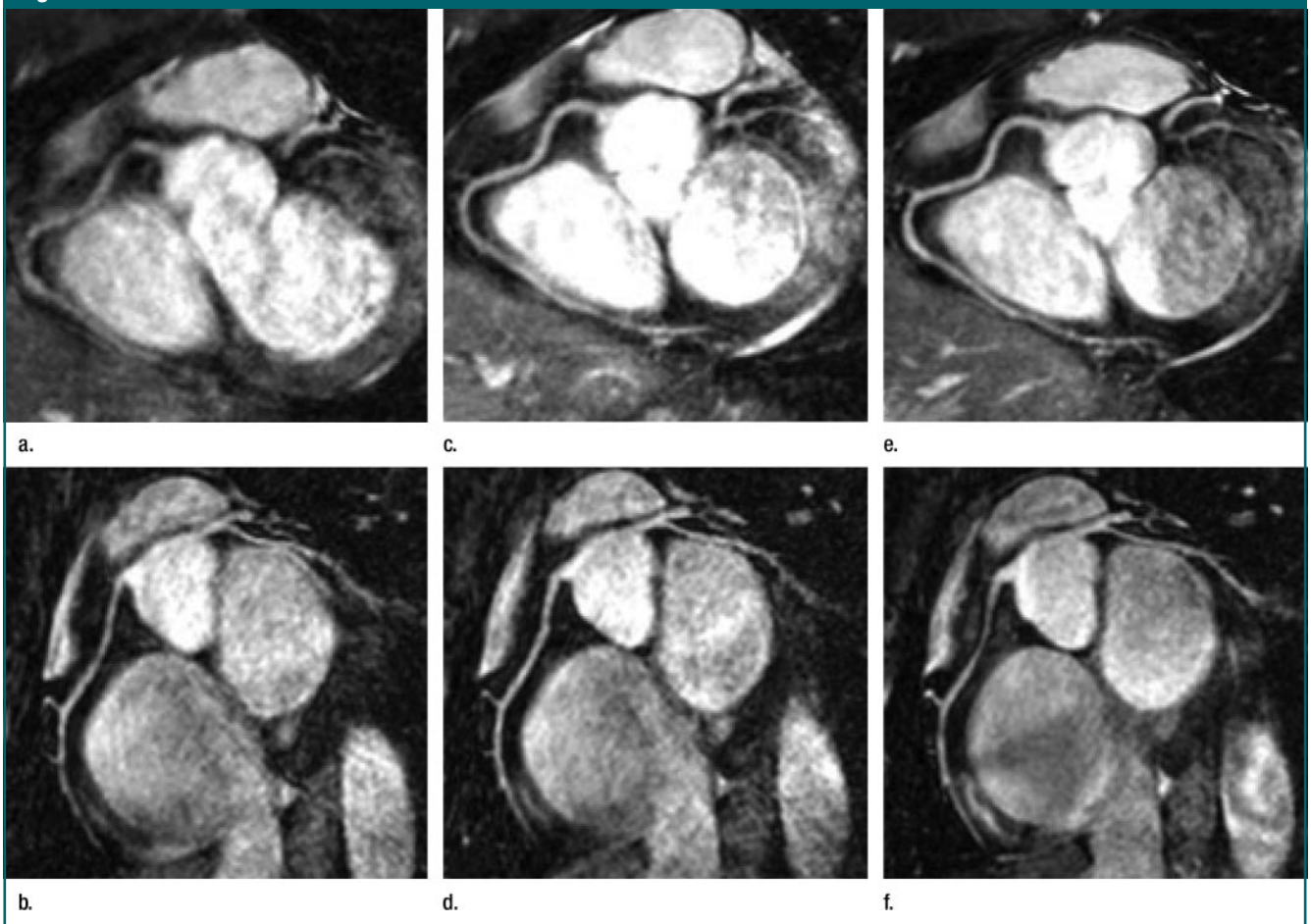

Figure 9: Reformatted MR images of right coronary arteries in two volunteers. Images were acquired with **(a, c, e)** Cartesian sequence and **(b, d, f)** spiral sequence. Images were acquired with **(a, b)** simple section tracking and 20-mm gating window; **(c, d)** 20-mm gating window and prospective correction with calibrated affine model, resulting in markedly improved image quality; and **(e, f)** 5-mm gating window and simple section tracking, requiring substantially increased acquisition time when compared with **a–d**. (Reprinted, with permission, from reference 149.)

ters may be used to correct for respiratory-induced deformation of the cardiac anatomy.

Subject-specific parameters are usually determined in a low-resolution prescan by using either multiple guided breath holds (147,148) or free breathing (144,149,151). The multiple images acquired at different respiratory positions are registered to one image selected as a reference, typically by using a block-matching technique, to determine the elements of the transformation matrix. In the case of a single navigator (147), simple linear regression may be used; if multiple navigators are used in different anatomic locations, more complex techniques—typically Gauss-Newton optimization—are used to relate the navigator information to the transformation parameters (148). Prospective image correction requires real-time modulation of the gradients used and, in the case of non-Cartesian imaging, the radiofrequency waveform (149) (Fig 9).

Jahnke et al (151) compared conventional angiography and a whole-heart 3D affine-corrected MR technique with navigators on the chest wall and right hemidiaphragm, a 10-mm gating window, and a patient-specific cardiac acquisition window. They demonstrated sensitivity, specificity, and diagnostic accuracy of 78%, 91%, and 89%, respectively, for detection of a stenosis of 50% or greater by using a 16-segment model where 424 of 512 coronary artery segments were considered evaluable. Manke et al (148) introduced the concept of the precursory navigator, which is an additional navigator echo collected some time earlier in the cardiac cycle than the main navigator, enabling correction for hysteretic deformation. In tests on a moving phantom, this technique was demonstrated to reduce motion-induced blurring in the circumferential direction (149). Inclusion

of the square of the navigator position (a quadratic navigator) in the model also reduced blurring in the radial direction in the same tests, and both modifications were found to reduce ghosting. In an extension to this work, Fischer et al (146) used the precursory navigators and a 2D subject-specific affine model and demonstrated respiratory efficiencies around 30% greater and a similar level of residual coronary motion with a 10-mm gating window, as compared with 2D subject-specific linear section tracking with the same navigators and a 5-mm window. Such techniques however, fix the motion model at the beginning of the acquisition and do not adapt to changes or short-term variability in the breathing pattern as the acquisition proceeds, which may cause problems over long imaging periods.

Table 5

Novel Techniques to Derive Motion Information from Low-Resolution Images or Aliased Subimages

Technique*	Image or Subimage Source for Respiratory Information	Original Application
	Low-Resolution MR Images from Center of k-Space	
Radial self-gating (159)	Fully sampled center of k-space from each radial interleaf pattern is reconstructed to form low-resolution images.	Cine MR acquisitions
PROPELLER (160)	Parallel readouts with incrementing angle for each interleaf are acquired, and fully sampled center of k-space is reconstructed to form low-resolution images (Fig 10)	Double-inversion dark-blood T2-weighted turbo spin-echo MR imaging
Variable-density adaptive averaging (65)	Spiral interleaves with higher density sampling in central k-space and lower density sampling further out are acquired, and a number of the higher density regions are reconstructed to form low-resolution images	Coronary artery MR imaging without ECG gating.
3D spiral fat navigator (161)	Selective excitation of fat around the heart with a low-resolution 3D stack of spiral readout data before main imaging interleaf (Fig 11).	Coronary vessel wall MR imaging
	Aliased Subimages from Sparsely Sampled k-Space	
BACSPIN (162)	Subimages reconstructed with heavy aliasing from every spiral interleaf in a segmented acquisition	Coronary MR angiography
Radial self-gating (163)	Subimages reconstructed from each radial interleaf	Balanced steady-state free precession MR imaging at end diastole

* Number in parentheses is the reference number. BACSPIN = breathing autocorrection with spiral interleaves, PROPELLER = periodically rotated overlapping parallel lines with enhanced reconstruction.

Figure 10

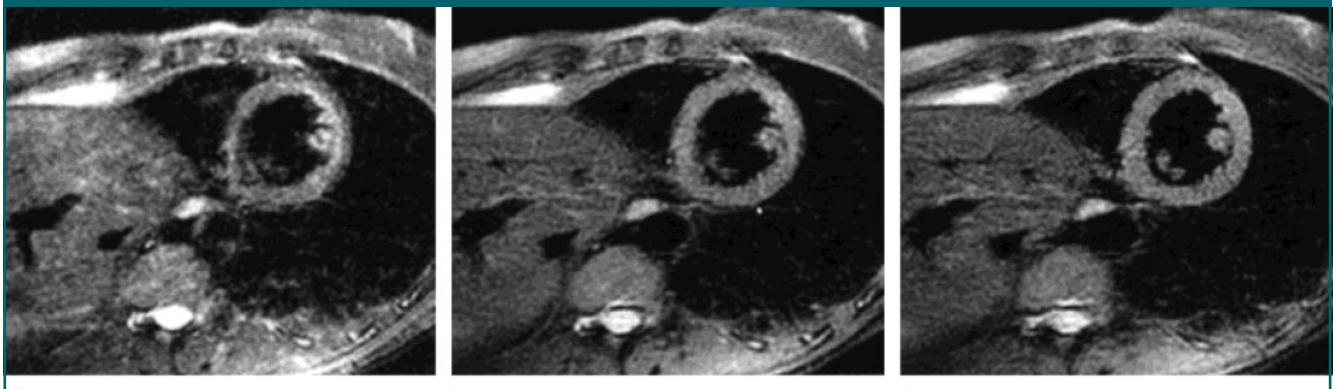

a. b. c.

Figure 10: Short-axis dark-blood–prepared T2-weighted turbo spin-echo MR images acquired in a healthy volunteer during free breathing: **(a)** conventional Cartesian acquisition, **(b)** with PROPELLER k-space trajectory and no motion correction, and **(c)** with PROPELLER trajectory and motion correction. (Adapted and reprinted, with permission, from reference 160.)

Figure 11

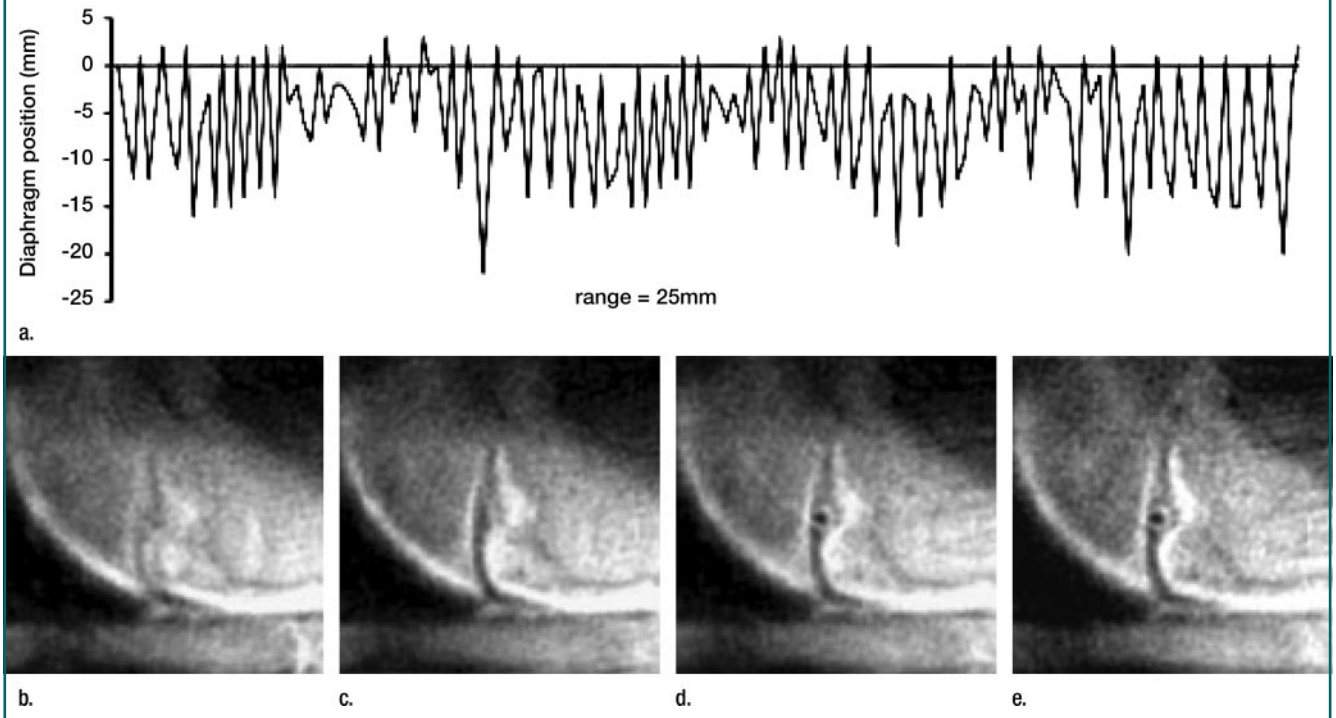

Figure 11: **(a)** Diaphragm trace and **(b–e)** dark-blood coronary MR images in a healthy volunteer acquired over full range of respiratory motion **(b)** with no motion correction and **(c–e)** after beat-to-beat correction of **(c)** in-plane motion in horizontal direction, **(d)** in-plane motion in horizontal and vertical directions, and **(e)** both in- and through-plane motion. **(a)** Diaphragm trace was monitored with a conventional right hemidiaphragmatic navigator throughout the acquisition. (Adapted and reprinted, with permission, from reference 161.)

Figure 12

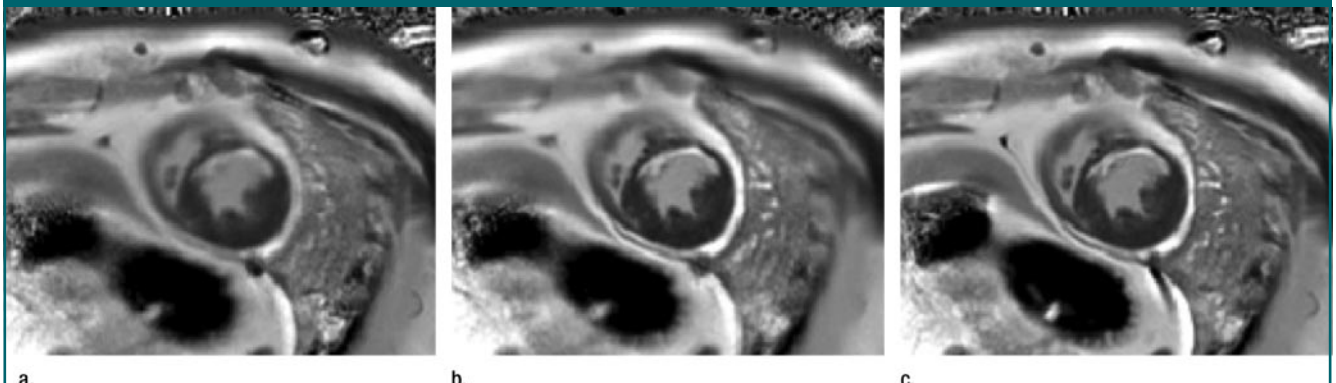

Figure 12: Delayed gadolinium-enhanced MR images in patient with chronic myocardial infarction. Images were acquired during free breathing and averaged over 30 frames with **(a)** no motion correction, **(b)** rigid body motion correction derived by registering user-defined region around LV in each image to same region in one frame used as reference, and **(c)** nonrigid motion correction derived by using automatic full field-of-view registration. (Adapted and reprinted, with permission, from reference 164.)

Image-based corrections and self-gating.—A number of motion-correction techniques have used parameters extracted from the imaging data set itself or from additionally acquired images rather than respiratory information derived from navigators or external devices. These techniques require no tracking factor because the respiratory motion is detected from the structure of interest itself.

In self-gating techniques, respira-

tory information is obtained from a one-dimensional projection of the heart repeatedly interleaved within the sequence (63,68,152–155). These techniques have been successfully applied to single-time-point (153) and to cine (155) and Cartesian (153) coronary artery imaging, as well as to radial cine acquisitions (67). Alternatively, multiple one-dimensional projections of the fat (156–158) around the heart have been used for coronary artery studies, resulting in equivalent or improved image quality when compared with simple diaphragmatic navigators.

Several methods involve reconstruction of low-resolution images from the fully sampled center of k-space, and these images are used to derive respiratory information (Table 5). This approach has been used for radial acquisitions (159), for PROPELLER acquisitions (Fig 10) (160), for variable-density spiral acquisitions (65), and for the 3D spiral fat navigator technique, which acquires a low-resolution volume with fat-selective excitation prior to the main imaging segment every R-R interval (161) (Fig 11).

Alternatively, for another group of techniques, respiratory information is derived from heavily aliased subimages that are reconstructed from an undersampled k-space (Table 5). These include breathing autocorrection with spiral interleaves, or BACSPIN (162), which uses spiral trajectories and a technique developed by McLeish et al (163) in which each undersampled interleave is reconstructed from a radial acquisition.

Another approach to motion correction is to use image-registration methods to correct motion between rapidly acquired images and potentially allow averaging to improve the signal-to-noise ratio. In adaptive averaging (64), which has been successfully used in coronary artery studies, a full image is generated every spiral or echo-planar interleaf by using a sliding window reconstruction and 2D motion information extracted and used to gate the acquisition or to register images before averaging. Similarly Ledesma-Carbayo et al (164) performed nonrigid registration and motion correction on a series of late-enhancement images acquired at a single time point in the cardiac cycle, before averaging (Fig 12). Automatic registration of the heart from image to image has also been used for short-axis cine imaging (165) and first-pass perfusion data acquired during free breathing (166–168), while Yang et al (169) used the phase difference between successive image frames to determine the translational shifts for the latter application.

Conclusion

The motion of the heart through the cardiac and respiratory cycles is complex and can result in blurring, ghosting, and misregistration artifacts in cardiovascular MR studies and can limit the resolution available. Gating techniques are generally used to reduce these artifacts to acceptable levels but result in prolonging the imaging time. While ECG gating with an acquisition window short enough to allow only acceptably low levels of motion is generally adequate for dealing with motion from the cardiac cycle, dealing with respiratory motion is more difficult. Breath holding can be applicable in some cases, but for high-temporal- or high-spatial-resolution studies or for those requiring higher signal-to-noise ratio, navigator-based gating or image-based registration is required.

Several methods of reducing the acquisition time while maintaining much of the image quality exist. Many of the more recently developed of these techniques do not rely on an inaccurate generalized model, and some include correction for nonrigid tissue deformation and hysteresis. This review has presented the methods currently available to enable high quality imaging during free breathing over a range of cardiovascular applications.

References

1. Schultz CL, Alfidi RJ, Nelson AD, Kopiwoda SY, Clampitt ME. The effect of motion on two-dimensional Fourier transformation magnetic resonance images. Radiology 1984;152:117–121.
2. Gatenby JC, McCauley TR, Gore JC. Mechanisms of signal loss in magnetic resonance imaging of stenoses. Med Phys 1993;20:1049–1057.
3. Firmin DN, Nayler GL, Kilner PJ, Longmore DB. The application of phase shifts in NMR for flow measurement. Magn Reson Med 1990;14:230–241.
4. Kilner PJ, Firmin DN, Rees RS, et al. Valve and great vessel stenosis: assessment with MR jet velocity mapping. Radiology 1991;178:229–235.
5. Nayler GL, Firmin DN, Longmore DB. Blood flow imaging by cine magnetic resonance. J Comput Assist Tomogr 1986;10:715–722.
6. Haacke EM, Lenz GW. Improving MR image quality in the presence of motion by using rephasing gradients. AJR Am J Roentgenol 1987;148:1251–1258.
7. Bradley WG. Carmen lecture: flow phenomena in MR imaging. AJR Am J Roentgenol 1988;150:983–994.
8. Mayo JR, Culham JA, MacKay AL, Aikins DG. Blood MR signal suppression by preexcitation with inverting pulses. Radiology 1989;173:269–271.
9. Edelman RR, Chien D, Kim D. Fast selective black blood MR imaging. Radiology 1991;181:655–660.
10. Lin HY, Dale BM, Flask CA, Duerk JL. Blood attenuation with SSFP-compatible saturation (BASS). J Magn Reson Imaging 2006;24:701–707.
11. Innes JA, Cort SC, Kox W, Guz A. Within-breath modulation of left ventricular function during normal breathing and positive-pressure ventilation in man. J Physiol 1993;460:487–502.
12. Thompson RB, McVeigh ER. Cardiorespiratory-resolved magnetic resonance imaging: measuring respiratory modulation of cardiac function. Magn Reson Med 2006;56:1301–1310.
13. Raper AJ, Richardson DW, Kontos HA, Patterson JL. Circulatory responses to breath holding in man. J Appl Physiol 1967;22:201–206.
14. Weissler AM, Harris WS, Schoenfeld CD. Systolic time intervals in heart failure in man. Circulation 1968;37:149–159.
15. Zerhouni EA, Parish DM, Rogers WJ, Yang A, Shapiro EP. Human heart: tagging with MR imaging—a method for noninvasive assessment of myocardial motion. Radiology 1988;169:59–63.
16. Axel L, Dougherty L. Heart wall motion: improved method of spatial modulation of

magnetization for MR imaging. Radiology 1989;172:349–350.

17. Axel L, Gonçalves RC, Bloomgarden D. Regional heart wall motion: two-dimensional analysis and functional imaging with MR imaging. Radiology 1992;183:745–750.
18. Petitjean C, Rougon N, Cluzel P. Assessment of myocardial function: a review of quantification methods and results using tagged MRI. J Cardiovasc Magn Reson 2005;7:501–516.
19. Axel L, Dougherty L. MR imaging of motion with spatial modulation of magnetization. Radiology 1989;171:841–845.
20. Azhari H, Weiss JL, Rogers WJ, Siu CO, Zerhouni EA, Shapiro EP. Noninvasive quantification of principal strains in normal canine hearts using tagged MRI images in 3-D. Am J Physiol 1993;264:H205–H216.
21. Guttman MA, Prince JL, McVeigh ER. Tag and contour detection in tagged MR images of the left ventricle. IEEE Trans Med Imaging 1994;13:74–88.
22. Kraitchman DL, Young AA, Chang CN, Axel L. Semi-automatic tracking of myocardial motion in MR tagged images. IEEE Trans Med Imaging 1995;14:422–433.
23. Kumar S, Goldgof D. Automatic tracking of SPAMM grid and the estimation of deformation parameters from cardiac MR images. IEEE Trans Med Imaging 1994;13:122–132.
24. Prince JL, McVeigh ER. Motion estimation from tagged MR image sequences. IEEE Trans Med Imaging 1992;11:238–249.
25. Osman NF, Kerwin WS, McVeigh ER, Prince JL. Cardiac motion tracking using CINE harmonic phase (HARP) magnetic resonance imaging. Magn Reson Med 1999;42:1048–1060.
26. Aletras AH, Ding S, Balaban RS, Wen H. DENSE: displacement encoding with stimulated echoes in cardiac functional MRI. J Magn Reson 1999;137:247–252.
27. Hoffman EA, Ritman EL. Invariant total heart volume in the intact thorax. Am J Physiol 1985;249:H883–H890.
28. Karwatowski SP, Mohiaddin R, Yang GZ, et al. Assessment of regional left ventricular long-axis motion with MR velocity mapping in healthy subjects. J Magn Reson Imaging 1994;4:151–155.
29. Karwatowski SP, Brecker SJ, Yang GZ, Firmin DN, Sutton MS, Underwood SR. A comparison of left ventricular myocardial velocity in diastole measured by magnetic resonance and left ventricular filling measured by Doppler echocardiography. Eur Heart J 1996;17:795–802.
30. Kvitting JP, Ebbers T, Engvall J, Sutherland GR, Wranne B, Wigström L. Three-directional myocardial motion assessed using 3D phase contrast MRI. J Cardiovasc Magn Reson 2004;6:627–636.
31. Petersen SE, Jung BA, Wiesmann F, et al. Myocardial tissue phase mapping with cine phase-contrast MR imaging: regional wall motion analysis in healthy volunteers. Radiology 2006;238:816–826.
32. Hennig J, Schneider B, Peschl S, Markl M, Krause T, Laubenberger J. Analysis of myocardial motion based on velocity measurements with a black blood prepared segmented gradient-echo sequence: methodology and applications to normal volunteers and patients. J Magn Reson Imaging 1998;8:868–877.
33. Arai AE, Gaither CC, Epstein FH, Balaban RS, Wolff SD. Myocardial velocity gradient imaging by phase contrast MRI with application to regional function in myocardial ischemia. Magn Reson Med 1999;42:98–109.
34. Markl M, Schneider B, Hennig J, et al. Cardiac phase contrast gradient echo MRI: measurement of myocardial wall motion in healthy volunteers and patients. Int J Card Imaging 1999;15:441–452.
35. Jung B, Schneider B, Markl M, Saurbier B, Geibel A, Hennig J. Measurement of left ventricular velocities: phase contrast MRI velocity mapping versus tissue-Doppler-ultrasound in healthy volunteers. J Cardiovasc Magn Reson 2004;6:777–783.
36. Jung B, Föll D, Böttler P, Petersen S, Hennig J, Markl M. Detailed analysis of myocardial motion in volunteers and patients using high-temporal-resolution MR tissue phase mapping. J Magn Reson Imaging 2006;24:1033–1039.
37. Haber I, Metaxas DN, Geva T, Axel L. Three-dimensional systolic kinematics of the right ventricle. Am J Physiol Heart Circ Physiol 2005;289:H1826–H1833.
38. Al-Kwifi O, Stainsby J, Foltz WD, Sussman MS, Huang Y, Wright GA. Characterizing coronary motion and its effect on MR coronary angiography: initial experience. J Magn Reson Imaging 2006;24:842–850.
39. Hofman MB, Wickline SA, Lorenz CH. Quantification of in-plane motion of the coronary arteries during the cardiac cycle: implications for acquisition window duration for MR flow quantification. J Magn Reson Imaging 1998;8:568–576.
40. Wang Y, Vidan E, Bergman GW. Cardiac motion of coronary arteries: variability in the rest period and implications for coronary MR angiography. Radiology 1999;213:751–758.
41. Kim WY, Stuber M, Kissinger KV, Andersen NT, Manning WJ, Botnar RM. Impact of bulk cardiac motion on right coronary MR angiography and vessel wall imaging. J Magn Reson Imaging 2001;14:383–390.
42. Jahnke C, Paetsch I, Nehrke K, et al. A new approach for rapid assessment of the cardiac rest period for coronary MRA. J Cardiovasc Magn Reson 2005;7:395–399.
43. Jahnke C, Paetsch I, Achenbach S, et al. Coronary MR imaging: breath-hold capability and patterns, coronary artery rest periods, and β-blocker use. Radiology 2006;239(1):71–78.
44. Holland AE, Goldfarb JW, Edelman RR. Diaphragmatic and cardiac motion during suspended breathing: preliminary experience and implications for breath-hold MR imaging. Radiology 1998;209:483–489.
45. Wang Y, Riederer SJ, Ehman RL. Respiratory motion of the heart: kinematics and the implications for the spatial resolution in coronary imaging. Magn Reson Med 1995;33:713–719.
46. Nehrke K, Börnert P, Manke D, Böck JC. Free-breathing cardiac MR imaging: study of implications of respiratory motion-initial results. Radiology 2001;220:810–815.
47. Taylor AM, Keegan J, Jhooti P, Firmin DN, Pennell DJ. Calculation of a subject-specific adaptive motion-correction factor for improved real-time navigator echo-gated magnetic resonance coronary angiography. J Cardiovasc Magn Reson 1999;1:131–138.
48. Taylor AM, Jhooti P, Wiesmann F, Keegan J, Firmin DN, Pennell DJ. MR navigator-echo monitoring of temporal changes in diaphragm position: implications for MR coronary angiography. J Magn Reson Imaging 1997;7:629–636.
49. McLeish K, Hill DL, Atkinson D, Blackall JM, Razavi R. A study of the motion and deformation of the heart due to respiration. IEEE Trans Med Imaging 2002;21:1142–1150.
50. Shechter G, Ozturk C, Resar JR, McVeigh ER. Respiratory motion of the heart from free breathing coronary angiograms. IEEE Trans Med Imaging 2004;23:1046–1056.
51. Serfaty JM, Yang X, Aksit P, Quick HH, Solaiyappan M, Atalar E. Toward MRI-guided coronary catheterization: visualization of guiding catheters, guidewires, and

anatomy in real time. J Magn Reson Imaging 2000;12:590–594.

52. Razavi R, Hill DL, Keevil SF, et al. Cardiac catheterisation guided by MRI in children and adults with congenital heart disease. Lancet 2003;362:1877–1882.

53. Zhang S, Rafie S, Chen Y, et al. In vivo cardiovascular catheterization under real-time MRI guidance. J Magn Reson Imaging 2006;24:914–917.

54. Yang PC, Kerr AB, Liu AC, et al. New real-time interactive cardiac magnetic resonance imaging system complements echocardiography. J Am Coll Cardiol 1998;32:2049–2056.

55. Pat GT, Pauly JM, Hu BS, Nishimura DG. One-shot spatially resolved velocity imaging. Magn Reson Med 1998;40:603–613.

56. Nayak KS, Pauly JM, Kerr AB, Hu BS, Nishimura DG. Real-time color flow MRI. Magn Reson Med 2000;43:251–258.

57. Macgowan CK, Kellenberger CJ, Detsky JS, Roman K, Yoo SJ. Real-time Fourier velocity encoding: an in vivo evaluation. J Magn Reson Imaging 2005;21:297–304.

58. de la Pena E, Nguyen PK, Nayak KS, et al. Real-time color-flow CMR in adults with congenital heart disease. J Cardiovasc Magn Reson 2006;8:809–815.

59. Denslow S, Buckles DS. Pulse oximetry-gated acquisition of cardiac MR images in patients with congenital cardiac abnormalities. AJR Am J Roentgenol 1993;160:831–833.

60. Lanzer P, Botvinick EH, Schiller NB, et al. Cardiac imaging using gated magnetic resonance. Radiology 1984;150:121–127.

61. Soulen RL, Higgins CB. Magnetic resonance imaging of the cardiovascular system. Magn Reson Annu 1985; 27–43.

62. Spraggins TA. Wireless retrospective gating: application to cine cardiac imaging. Magn Reson Imaging 1990;8:675–681.

63. Kim WS, Mun CW, Kim DJ, Cho ZH. Extraction of cardiac and respiratory motion cycles by use of projection data and its applications to NMR imaging. Magn Reson Med 1990;13:25–37.

64. Hardy CJ, Saranathan M, Zhu Y, Darrow RD. Coronary angiography by real-time MRI with adaptive averaging. Magn Reson Med 2000;44:940–946.

65. Sussman MS, Stainsby JA, Robert N, Merchant N, Wright GA. Variable-density adaptive imaging for high-resolution coronary artery MRI. Magn Reson Med 2002;48:753–764.

66. Crowe ME, Larson AC, Zhang Q, et al. Automated rectilinear self-gated cardiac cine imaging. Magn Reson Med 2004;52:782–788.

67. Larson AC, White RD, Laub G, McVeigh ER, Li D, Simonetti OP. Self-gated cardiac cine MRI. Magn Reson Med 2004;51:93–102.

68. Brau AC, Brittain JH. Generalized self-navigated motion detection technique: Preliminary investigation in abdominal imaging. Magn Reson Med 2006;55:263–270.

69. Fischer SE, Wickline SA, Lorenz CH. Novel real-time R-wave detection algorithm based on the vectorcardiogram for accurate gated magnetic resonance acquisitions. Magn Reson Med 1999;42(2):361–370.

70. Leiner T, Katsimaglis G, Yeh EN, et al. Correction for heart rate variability improves coronary magnetic resonance angiography. J Magn Reson Imaging 2005;22:577–582.

71. Bluemke DA, Boxerman JL, Atalar E, McVeigh ER. Segmented k-space cine breath-hold cardiovascular MR imaging. I. Principles and technique. AJR Am J Roentgenol 1997;169:395–400.

72. Sievers B, Addo M, Kirchberg S, et al. Impact of the ECG gating method on ventricular volumes and ejection fractions assessed by cardiovascular magnetic resonance imaging. J Cardiovasc Magn Reson 2005;7:441–446.

73. Lenz GW, Haacke EM, White RD. Retrospective cardiac gating: a review of technical aspects and future directions. Magn Reson Imaging 1989;7:445–455.

74. Sievers B, Addo M, Kirchberg S, et al. How much are atrial volumes and ejection fractions assessed by cardiac magnetic resonance imaging influenced by the ECG gating method? J Cardiovasc Magn Reson 2005;7:587–593.

75. Hofman MB, van Rossum AC, Sprenger M, Westerhof N. Assessment of flow in the right human coronary artery by magnetic resonance phase contrast velocity measurement: effects of cardiac and respiratory motion. Magn Reson Med 1996;35:521–531.

76. Duerinckx A, Atkinson DP. Coronary MR angiography during peak-systole: work in progress. J Magn Reson Imaging 1997;7:979–986.

77. Stuber M, Botnar RM, Danias PG, Kissinger KV, Manning WJ. Submillimeter three-dimensional coronary MR angiography with real-time navigator correction: comparison of navigator locations. Radiology 1999;212:579–587.

78. Wang Y, Watts R, Mitchell I, et al. Coronary MR angiography: selection of acquisition window of minimal cardiac motion with electrocardiography-triggered navigator cardiac motion prescanning—initial results. Radiology 2001;218(2):580–585.

79. Plein S, Jones TR, Ridgway JP, Sivananthan MU. Three-dimensional coronary MR angiography performed with subject-specific cardiac acquisition windows and motion-adapted respiratory gating. AJR Am J Roentgenol 2003;180:505–512.

80. Roes SD, Korosoglou G, Schär M, et al. Correction for heart rate variability during 3D whole heart MR coronary angiography. J Magn Reson Imaging 2008;27:1046–1053.

81. Wang Y, Ehman RL. Retrospective adaptive motion correction for navigator-gated 3D coronary MR angiography. J Magn Reson Imaging 2000;11:208–214.

82. Stehning C, Börnert P, Nehrke K, Dössel O. Free breathing 3D balanced FFE coronary magnetic resonance angiography with prolonged cardiac acquisition windows and intra-RR motion correction. Magn Reson Med 2005;53:719–723.

83. Simonetti OP, Finn JP, White RD, Laub G, Henry DA. "Black blood" T2-weighted inversion-recovery MR imaging of the heart. Radiology 1996;199:49–57.

84. Keegan J, Gatehouse PD, Prasad SK, Firmin DN. Improved turbo spin-echo imaging of the heart with motion-tracking. J Magn Reson Imaging 2006;24(3):563–570.

85. Kozerke S, Scheidegger MB, Pedersen EM, Boesiger P. Heart motion adapted cine phase-contrast flow measurements through the aortic valve. Magn Reson Med 1999;42:970–978.

86. Kozerke S, Schwitter J, Pedersen EM, Boesiger P. Aortic and mitral regurgitation: quantification using moving slice velocity mapping. J Magn Reson Imaging 2001;14:106–112.

87. Dowsey AW, Keegan J, Lerotic M, Thom S, Firmin D, Yang GZ. Motion-compensated MR valve imaging with COMB tag tracking and super-resolution enhancement. Med Image Anal 2007;11:478–491.

88. Dowsey AW, Keegan J, Yang GZ. Cardiac-motion compensated MR imaging and strain analysis of ventricular trabeculae. In: Proceedings of the 10th International Conference on Medical Image Computing and Computer-Assisted Intervention—MICCAI.

Berlin, Germany: Springer-Verlag, 2007; 609–616.

89. Dumoulin CL, Doorly DJ, Caro CG. Quantitative measurement of velocity at multiple positions using comb excitation and Fourier velocity encoding. Magn Reson Med 1993; 29:44–52.
90. Fischer SE, McKinnon GC, Scheidegger MB, Prins W, Meier D, Boesiger P. True myocardial motion tracking. Magn Reson Med 1994;31:401–413.
91. Kayser HW, Stoel BC, van der Wall EE, van der Geest RJ, de Roos A. MR velocity mapping of tricuspid flow: correction for through-plane motion. J Magn Reson Imaging 1997;7:669–673.
92. Sakuma H, Blake LM, Amidon TM, et al. Coronary flow reserve: noninvasive measurement in humans with breath-hold velocity-encoded cine MR imaging. Radiology 1996;198:745–750.
93. Marcus JT, Smeenk HG, Kuijer JP, der Geest RJ, Heethaar RM, Rossum AC. Flow profiles in the left anterior descending and the right coronary artery assessed by MR velocity quantification: effects of through-plane and in-plane motion of the heart. J Comput Assist Tomogr 1999;23:567–576.
94. Keegan J, Gatehouse PD, Yang GZ, Firmin DN. Spiral phase velocity mapping of left and right coronary artery blood flow: correction for through-plane motion using selective fat-only excitation. J Magn Reson Imaging 2004;20:953–960.
95. Steiner RE, Bydder GM, Selwyn A, et al. Nuclear magnetic resonance imaging of the heart: current status and future prospects. Br Heart J 1983;50:202–208.
96. Alfidi RJ, Haaga JR, El-Yousef SJ, et al. Preliminary experimental results in humans and animals with a superconducting, whole-body, nuclear magnetic resonance scanner. Radiology 1982;143:175–181.
97. Higgins CB, Byrd BF, McNamara MT, et al. Magnetic resonance imaging of the heart: a review of the experience in 172 subjects. Radiology 1985;155:671–679.
98. Atkinson DJ, Edelman RR. Cineangiography of the heart in a single breath hold with a segmented turboFLASH sequence. Radiology 1991;178:357–360.
99. Sakuma H, Kawada N, Kubo H, et al. Effect of breath holding on blood flow measurement using fast velocity encoded cine MRI. Magn Reson Med 2001;45:346–348.
100. Feinberg DA, Rofsky NM, Johnson G. Multiple breath-hold averaging (MBA) method for increased SNR in abdominal MRI. Magn Reson Med 1995;34:905–909.
101. Noble NM, Boubertakh R, Razavi RS, Hill DL. Inter-breath-hold registration for the production of high resolution cardiac MR volumes. Med Image Comput Comput Assist Interv Int Conf Med Image Comput Comput Assist Interv 2005;8:894–901.
102. McCarthy RM, Shea SM, Deshpande VS, et al. Coronary MR angiography: true FISP imaging improved by prolonging breath holds with preoxygenation in healthy volunteers. Radiology 2003;227:283–288.
103. Danias PG, Stuber M, Botnar RM, Kissinger KV, Edelman RR, Manning WJ. Relationship between motion of coronary arteries and diaphragm during free breathing: lessons from real-time MR imaging. AJR Am J Roentgenol 1999;172:1061–1065.
104. Marks B, Mitchell DG, Simelaro JP. Breath-holding in healthy and pulmonary-compromised populations: effects of hyperventilation and oxygen inspiration. J Magn Reson Imaging 1997;7:595–597.
105. Danias PG, Stuber M, Botnar RM, Kissinger KV, Chuang ML, Manning WJ. Navigator assessment of breath-hold duration: impact of supplemental oxygen and hyperventilation. AJR Am J Roentgenol 1998;171:395–397.
106. Ehman RL, McNamara MT, Pallack M, Hricak H, Higgins CB. Magnetic resonance imaging with respiratory gating: techniques and advantages. AJR Am J Roentgenol 1984;143:1175–1182.
107. Felblinger J, Boesch C. Amplitude demodulation of the electrocardiogram signal (ECG) for respiration monitoring and compensation during MR examinations. Magn Reson Med 1997;38:129–136.
108. Wang Y, Christy PS, Korosec FR, et al. Coronary MRI with a respiratory feedback monitor: the 2D imaging case. Magn Reson Med 1995;33:116–121.
109. McConnell MV, Khasgiwala VC, Savord BJ, et al. Comparison of respiratory suppression methods and navigator locations for MR coronary angiography. AJR Am J Roentgenol 1997;168:1369–1375.
110. Bailes DR, Gilderdale DJ, Bydder GM, Collins AG, Firmin DN. Respiratory ordered phase encoding (ROPE): a method for reducing respiratory motion artifacts in MR imaging. J Comput Assist Tomogr 1985;9:835–838.
111. Feinburg DA, Bongers A, Ramanna S, Guenther M. Real-time ultrasound imaging in MRI scanner for guidance of cardiac MR [abstr]. In: Proceedings of the 15th Meeting of the International Society for Magnetic Resonance in Medicine. Berkeley, Calif: International Society for Magnetic Resonance in Medicine, 2007; 3861.
112. Danias PG, McConnell MV, Khasgiwala VC, Chuang ML, Edelman RR, Manning WJ. Prospective navigator correction of image position for coronary MR angiography. Radiology 1997;203:733–736.
113. Ehman RL, Felmlee JP. Adaptive technique for high-definition MR imaging of moving structures. Radiology 1989;173:255–263.
114. Liu YL, Riederer SJ, Rossman PJ, Grimm RC, Debbins JP, Ehman RL. A monitoring, feedback, and triggering system for reproducible breath-hold MR imaging. Magn Reson Med 1993;30:507–511.
115. Wang Y, Grimm RC, Felmlee JP, Riederer SJ, Ehman RL. Algorithms for extracting motion information from navigator echoes. Magn Reson Med 1996;36:117–123.
116. Du YP, Saranathan M, Foo TK. An accurate, robust, and computationally efficient navigator algorithm for measuring diaphragm positions. J Cardiovasc Magn Reson 2004;6:483–490.
117. Stuber M, Botnar RM, Spuentrup E, Kissinger KV, Manning WJ. Three-dimensional high-resolution fast spin-echo coronary magnetic resonance angiography. Magn Reson Med 2001;45:206–211.
118. Spuentrup E, Manning WJ, Botnar RM, Kissinger KV, Stuber M. Impact of navigator timing on free-breathing submillimeter 3D coronary magnetic resonance angiography. Magn Reson Med 2002;47:196–201.
119. Li D, Kaushikkar S, Haacke EM, et al. Coronary arteries: three-dimensional MR imaging with retrospective respiratory gating. Radiology 1996;201:857–863.
120. Gatehouse PD, Keegan J, Yang GZ, Mohiaddin RH, Firmin DN. Tracking local volume 3D-echo-planar coronary artery imaging. Magn Reson Med 2001;46:1031–1036.
121. Wang Y, Rossman PJ, Grimm RC, Riederer SJ, Ehman RL. Navigator-echo-based real-time respiratory gating and triggering for reduction of respiration effects in three-dimensional coronary MR angiography. Radiology 1996;198:55–60.
122. Chandler AG, Pinder RJ, Netsch T, et al. Correction of misaligned slices in multi-slice cardiovascular magnetic resonance using slice-to-volume registration. J Cardiovasc Magn Reson 2008;10:13.
123. Taylor AM, Jhooti P, Keegan J, Simonds AK, Pennell DJ. Magnetic resonance navigator echo diaphragm monitoring in patients with suspected diaphragm paralysis. J Magn Reson Imaging 1999;9:69–74.

124. Sachs TS, Meyer CH, Hu BS, Kohli J, Nishimura DG, Macovski A. Real-time motion detection in spiral MRI using navigators. Magn Reson Med 1994;32:639–645.

125. Oshinski JN, Hofland L, Mukundan S, Dixon WT, Parks WJ, Pettigrew RI. Two-dimensional coronary MR angiography without breath holding. Radiology 1996; 201:737–743.

126. Maki JH, Prince MR, Londy FJ, Chenevert TL. The effects of time varying intravascular signal intensity and k-space acquisition order on three-dimensional MR angiography image quality. J Magn Reson Imaging 1996;6:642–651.

127. Haacke EM, Patrick JL. Reducing motion artifacts in two-dimensional Fourier transform imaging. Magn Reson Imaging 1986;4: 359–376.

128. Jhooti P, Wiesmann F, Taylor AM, et al. Hybrid ordered phase encoding (HOPE): an improved approach for respiratory artifact reduction. J Magn Reson Imaging 1998; 8:968–980.

129. Jhooti P, Keegan J, Gatehouse PD, et al. 3D coronary artery imaging with phase reordering for improved scan efficiency. Magn Reson Med 1999;41:555–562.

130. Sachs TS, Meyer CH, Irarrazabal P, Hu BS, Nishimura DG, Macovski A. The diminishing variance algorithm for real-time reduction of motion artifacts in MRI. Magn Reson Med 1995;34:412–422.

131. Sachs TS, Meyer CH, Pauly JM, Hu BS, Nishimura DG, Macovski A. The real-time interactive 3-D-DVA for robust coronary MRA. IEEE Trans Med Imaging 2000;19: 73–79.

132. Weiger M, Börnert P, Proksa R, Schäffter T, Haase A. Motion-adapted gating based on k-space weighting for reduction of respiratory motion artifacts. Magn Reson Med 1997;38:322–333.

133. Sinkus R, Börnert P. Motion pattern adapted real-time respiratory gating. Magn Reson Med 1999;41:148–155.

134. Hackenbroch M, Nehrke K, Gieseke J, et al. 3D motion adapted gating (3D MAG): a new navigator technique for accelerated acquisition of free breathing navigator gated 3D coronary MR-angiography. Eur Radiol 2005;15:1598–1606.

135. Langreck H, Schnackenburg B, Nehrke K, et al. MR coronary artery imaging with 3D motion adapted gating (MAG) in comparison to a standard prospective navigator technique. J Cardiovasc Magn Reson 2005; 7:793–797.

136. Korin HW, Felmlee JP, Ehman RL, Riederer SJ. Adaptive technique for three-dimensional MR imaging of moving structures. Radiology 1990;177:217–221.

137. McConnell MV, Khasgiwala VC, Savord BJ, et al. Prospective adaptive navigator correction for breath-hold MR coronary angiography. Magn Reson Med 1997;37:148–152.

138. Weber OM, Martin AJ, Higgins CB. Whole-heart steady-state free precession coronary artery magnetic resonance angiography. Magn Reson Med 2003;50:1223–1228.

139. Börnert P, Aldefeld B, Nehrke K. Improved 3D spiral imaging for coronary MR angiography. Magn Reson Med 2001;45:172–175.

140. Oshinski JN, Hofland L, Dixon WT, Pettigrew RI. Magnetic resonance coronary angiography using navigator echo gated real-time slice following. Int J Card Imaging 1998;14:191–199.

141. Botnar RM, Stuber M, Kissinger KV, Kim WY, Spuentrup E, Manning WJ. Noninvasive coronary vessel wall and plaque imaging with magnetic resonance imaging. Circulation 2000;102:2582–2587.

142. Keegan J, Gatehouse P, Yang GZ, Firmin D. Coronary artery motion with the respiratory cycle during breath-holding and free-breathing: implications for slice-followed coronary artery imaging. Magn Reson Med 2002;47:476–481.

143. Nagel E, Bornstedt A, Schnackenburg B, Hug J, Oswald H, Fleck E. Optimization of realtime adaptive navigator correction for 3D magnetic resonance coronary angiography. Magn Reson Med 1999;42:408–411.

144. Manke D, Nehrke K, Börnert P, Rösch P, Dössel O. Respiratory motion in coronary magnetic resonance angiography: a comparison of different motion models. J Magn Reson Imaging 2002;15:661–671.

145. Yang GZ, Gatehouse PD, Keegan J, Mohiaddin RH, Firmin DN. Three-dimensional coronary MR angiography using zonal echo planar imaging. Magn Reson Med 1998;39:833–842.

146. Fischer RW, Botnar RM, Nehrke K, Boesiger P, Manning WJ, Peters DC. Analysis of residual coronary artery motion for breath hold and navigator approaches using real-time coronary MRI. Magn Reson Med 2006;55:612–618.

147. Manke D, Rösch P, Nehrke K, Börnert P, Dössel O. Model evaluation and calibration for prospective respiratory motion correction in coronary MR angiography based on 3-D image registration. IEEE Trans Med Imaging 2002;21:1132–1141.

148. Manke D, Nehrke K, Börnert P. Novel prospective respiratory motion correction approach for free-breathing coronary MR angiography using a patient-adapted affine motion model. Magn Reson Med 2003;50: 122–131.

149. Nehrke K, Börnert P. Prospective correction of affine motion for arbitrary MR sequences on a clinical scanner. Magn Reson Med 2005;54:1130–1138.

150. Jahnke C, Nehrke K, Paetsch I, et al. Improved bulk myocardial motion suppression for navigator-gated coronary magnetic resonance imaging. J Magn Reson Imaging 2007;26:780–786.

151. Jahnke C, Paetsch I, Nehrke K, et al. Rapid and complete coronary arterial tree visualization with magnetic resonance imaging: feasibility and diagnostic performance. Eur Heart J 2005;26:2313–2319.

152. Stehning C, Börnert P, Nehrke K, Eggers H, Stuber M. Free-breathing whole-heart coronary MRA with 3D radial SSFP and self-navigated image reconstruction. Magn Reson Med 2005;54:476–480.

153. Uribe S, Muthurangu V, Boubertakh R, et al. Whole-heart cine MRI using real-time respiratory self-gating. Magn Reson Med 2007;57:606–613.

154. Spincemaille P, Nguyen TD, Prince MR, Wang Y. Kalman filtering for real-time navigator processing. Magn Reson Med 2008; 60:158–168.

155. Lai P, Larson AC, Park J, Carr JC, Li D. Respiratory self-gated four-dimensional coronary MR angiography: a feasibility study. Magn Reson Med 2008;59:1378–1385.

156. Nguyen TD, Nuval A, Mulukutla S, Wang Y. Direct monitoring of coronary artery motion with cardiac fat navigator echoes. Magn Reson Med 2003;50:235–241.

157. Nguyen TD, Spincemaille P, Prince MR, Wang Y. Cardiac fat navigator-gated steady-state free precession 3D magnetic resonance angiography of coronary arteries. Magn Reson Med 2006;56:210–215.

158. Nguyen TD, Spincemaille P, Weinsaft JW, et al. A fast navigator-gated 3D sequence for delayed enhancement MRI of the myocardium: comparison with breathhold 2D imaging. J Magn Reson Imaging 2008; 27:802–808.

159. Larson AC, Kellman P, Arai A, et al. Preliminary investigation of respiratory self-gating for free-breathing segmented cine MRI. Magn Reson Med 2005;53:159–168.

160. Pipe JG. Motion correction with PROPELLER MRI: application to head motion and free-

breathing cardiac imaging. Magn Reson Med 1999;42:963–969.

161. Keegan J, Gatehouse PD, Yang GZ, Firmin DN. Non-model-based correction of respiratory motion using beat-to-beat 3D spiral fat-selective imaging. J Magn Reson Imaging 2007;26:624–629.

162. Hardy CJ, Zhao L, Zong X, Saranathan M, Yucel EK. Coronary MR angiography: respiratory motion correction with BACSPIN. J Magn Reson Imaging 2003;17:170–176.

163. McLeish K, Kozerke S, Crum WR, Hill DL. Free-breathing radial acquisitions of the heart. Magn Reson Med 2004;52:1127–1135.

164. Ledesma-Carbayo MJ, Kellman P, Arai AE, McVeigh ER. Motion corrected free-breathing delayed-enhancement imaging of myocardial infarction using nonrigid registration. J Magn Reson Imaging 2007;26:184–190.

165. Kellman P, Chefd'hotel C, Lorenz CH, Mancini C, Arai AE, McVeigh ER. Fully automatic, retrospective enhancement of real-time acquired cardiac cine MR images using image-based navigators and respiratory motion-corrected averaging. Magn Reson Med 2008;59:771–778.

166. Bidaut LM, Vallée JP. Automated registration of dynamic MR images for the quantification of myocardial perfusion. J Magn Reson Imaging 2001;13:648–655.

167. Kawakami K, Murase K, Kumashiro M, et al. Automatic motion correction for quantification of myocardial perfusion with dynamic magnetic resonance imaging. Magn Reson Med Sci 2004;3:105–117.

168. Stegmann MB, Olafsdóttir H, Larsson HB. Unsupervised motion-compensation of multi-slice cardiac perfusion MRI. Med Image Anal 2005;9:394–410.

169. Yang GZ, Burger P, Panting J, et al. Motion and deformation tracking for short-axis echo-planar myocardial perfusion imaging. Med Image Anal 1998;2:285–302.